Fracture of Brittle, Disordered Materials

Concrete, Rock and Ceramics

Edited by

G. BAKER and B. L. KARIHALOO

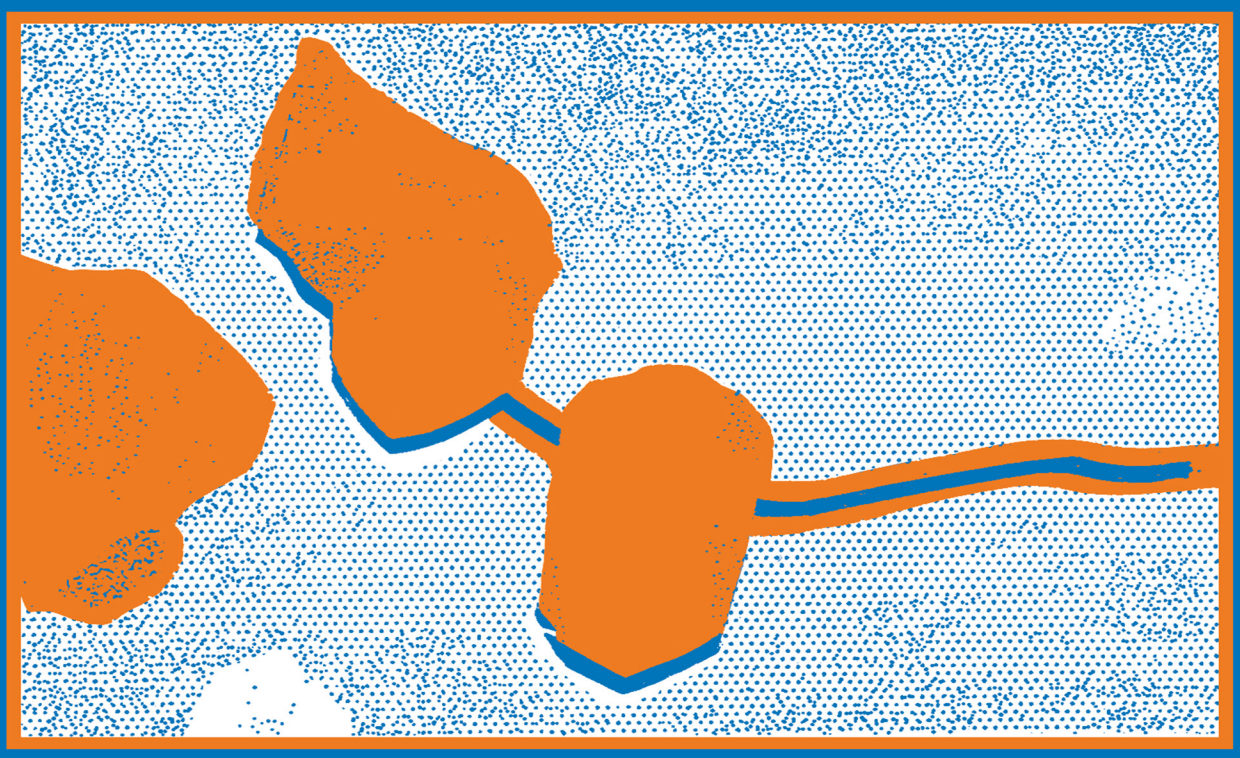

Taylor & Francis
Taylor & Francis Group

Fracture of Brittle, Disordered Materials

CONCRETE, ROCK AND CERAMICS

Fracture of Brittle, Disordered Materials

CONCRETE, ROCK AND CERAMICS

Proceedings of The International Union of Theoretical and Applied Mechanics (IUTAM) Symposium on Fracture of Brittle, Disordered Materials: Concrete, Rock and Ceramics, 20–24 September 1993, The University of Queensland, Brisbane, Australia

Edited by

G. BAKER
Department of Civil Engineering, The University of Queensland, Brisbane, Australia

and

B.L. KARIHALOO
Department of Civil and Mining Engineering, The University of Sydney, Sydney, Australia

Taylor & Francis
Taylor & Francis Group
LONDON AND NEW YORK

By Taylor & Francis,
2 Park Square, Milton Park, Abingdon, Oxon, OX14 4RN
270 Madison Ave, New York NY 10016

First edition 1995

Transferred to Digital Printing 2006

ISBN 0 419 19050 3

A catalogue record for this book is available from the British Library

Publisher's Note

This book has been produced from camera ready copy provided by the individual contributors.

The publisher has gone to great lengths to ensure the quality of this reprint but points out that some imperfections in the original may be apparent

Contents

Preface

One motivation for this conference was to bring together researchers from the concrete, rock and ceramics communities to seek common approaches to the study of fracture in these quasi-brittle materials. The intention then was to provide a blend of expertise in theoretical, computational and experimental mechanics, applied to different materials, to maximize dissemination of knowledge.

This concept proved very successful in several ways. Researchers were made aware of developments in other areas which could be transferred to their own; discussions on the nature of softening and the length of the damage/process zone and the mechanisms of toughening provided clear advances in this sense. Where approaches seemed quite distinct, positive benefit was derived from the reasons for the differences and the knowledge of the corresponding tradition; notable examples included the very definition of a process zone and relative crack tip, and hence the meaning of bridging forces, as well as the emphasis on crack growth versus strength considerations. There was undoubtedly common ground in numerical modelling, albeit with different objectives. Importantly, different experiences provided interesting challenges for computational modelling; the influence of crack closures and the loss of frictional cohesion due to sliding abrasions were raised as particular difficulties. Localization both in micromechanical and macroscopic modelling arose naturally as topics of current concern. Size and scale effects were prominent, with the inherent particle/grain sizes of the three materials being so different.

In following IUTAM's policy that all lectures should be invited, with full review of abstracts and final papers, the opportunity arose to programme for substantial presentations. The result was that discussion was always lively and incisive, and many new ideas were generated. In a slight departure from the norm, five posters were accepted from research students and recent post-doctoral researchers. These were summarized in a special session, and short papers are correspondingly published under a separate heading in these proceedings.

Financial support was generously provided by The International Union of Theoretical and Applied Mechanics (IUTAM) and the Department of Civil Engineering of The University of Queensland. There is no doubt that without this assistance we would not have been able to mount such an important scientific meeting, with the participation of so many active researchers and practitioners in the field. This financial support is greatly appreciated.

We believe that these proceedings will provide a useful basis for further and innovative research in the field of fracture of quasi-brittle materials. Many important issues were raised during the conference, some of which are consequently already under investigation. We hope that new scientists to the field might be motivated by topics discussed to instigate new lines of endeavour, and that fertilization across the discipline boundaries may continue to flourish.

We would like to thank the staff in the Department of Civil Engineering at The University of Queensland, and particularly graduate students Stefan Essebier and Lars Rassmussen, for their invaluable assistance throughout. We would like also to thank Professor E. T. Brown, Deputy Vice-Chancellor, for his wise and encouraging opening address. Finally, and perhaps most of all, we wish to thank the delegates who attended this meeting, many of whom came just to be involved in discussions.

Graham Baker
Bhushan Karihaloo

Brisbane, November 1993

Scientific Committee

G. Baker	*The University of Queensland, Australia*
B. L. Karihaloo	*The University of Sydney, Australia*
A. Carpinteri	*Politecnico di Torino, Italy*
L. Elfgren	*Luleå University, Sweden*
M. Elices	*Politecnica de Madrid, Spain*
P. Germain	*French Academy of Sciences, France*
D. Gross	*Darmstadt University, Germany*
H. Horii	*Tokyo University, Japan*
A. R. Ingraffea	*Cornell University, USA*
A. S. Kobayashi	*Washington University, USA*
Z. Mroz	*Polish Academy of Sciences, Poland*
J. G. M. van Mier	*Delft University of Technology, The Netherlands*

Countries represented and number of participants

Australia	38	Norway	1
Denmark	6	Poland	1
France	1	Singapore	1
Germany	3	Spain	2
Iran	1	Sweden	2
Italy	3	Switzerland	1
Japan	5	UK	4
Lichtenstein	1	USA	11
The Netherlands	6	**Total**	**87**

KEYNOTE ADDRESS

Chair: B.L. Karihaloo

1 THE SCALING LAWS AND RENORMALIZATION GROUP IN THE MECHANICS AND MICROMECHANICS OF FRACTURE

G.I. BARENBLATT
Department of Applied Mathematics and Theoretical Physics,
University of Cambridge, Cambridge, UK

Abstract
The concepts of scaling and self-similarity will be analyzed both from the viewpoints of the intermediate asymptotics, known in applied mathematics, and renormalization group, known in theoretical physics.

The general outline will be given of micromechanics, the branch of continuum mechanics studying the phenomena where the variations of the material microstructure are of governing influence on the macroscopic behaviour of bodies. Fracture is going on in zones of high stress concentration where the phenomenon is complicated by phase transformations, chemical transformations and heat generation. This makes natural the application of the micromechanical approach in the sense just mentioned to the fracture phenomenon, however the mathematical models become extremely complicated.

Examples will be presented of the application of intermediate asymptotics, scaling and renormalization group approach to constructing mechanical and micromechanical models of fracture phenomena. Special attention will be given to fatigue fracture phenomena, where these concepts simplify essentially mathematical models and lead to practically important quantitative relationships.

Keywords: Scaling, Self-similarity, Micromechanics, Fracture, Fatigue.

Fracture of Brittle Disordered Materials: Concrete, Rock and Ceramics. Edited by G. Baker and B.L. Karihaloo.
Published in 1995 by Taylor & Francis, 2 Park Square, Milton Park, Abingdon, Oxon, OX14 4RN. ISBN: 0 419 19050 3.

1 Introduction

The characteristic time of all kinetic processes in solids, including phase transformation and breaking of bonds between the elements of microstructure decreases very strongly, in fact exponentially, with growing tensile stresses. Therefore at the tips of the cracks where there is strong stress concentration fracture processes are usually complicated by microstructural transformations, heat generation and microscopic damage accumulation. It makes the traditional approach of mechanics based on constitutive equations sometimes insufficient. The approach of micromechanics seems to be more adequate, according to which the macroscopic equations of mechanics, and the equations of the kinetics of microstructural transformations and heat generation are considered simultaneously. Of course, it makes the mathematical models much more complicated. However, such tools as intermediate asymptotical approach, scaling and renormalization group could be helpful in constructing mathematical models. It is specially important for fatigue studies: fatigue now is one of the greatest challenges both for mathematicians and engineers.

2 Scaling, self-similarity, intermediate asymptotics

2.1 Example: J.J. Benbow conical crack

Benbow (1960) observed (Figure 1) a conical crack formed when

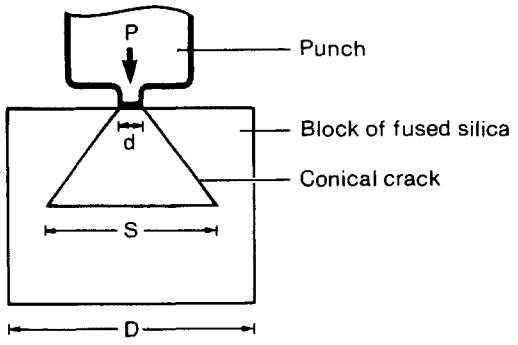

Fig. 1 Benbow conical crack (principal scheme)

a punch of small diameter d is penetrating under a load P into a block of fused silica having a large length-scale size D. From a general viewpoint it is clear that the diameter S of the base of this conical crack depends on the following quantities: P, d, D, Poisson ratio ν and cohesion modules K (here we deal with a stable crack, therefore the cohesion modulus, and not K_{IC} should be used). Dimensional analysis gives

$$S = (\frac{P}{K})^{2/3}\Phi(\nu, \frac{d}{(P/K)^{2/3}}, \frac{D}{(P/K)^{2/3}}) \tag{1}$$

Now we bear in mind that $D \gg d$ and, moreover, the diameter of the base S is much more that the diameter of the punch, but simultaneously, much less than D, so that

$$\frac{d}{(P/K)^{2/3}} \ll 1, \frac{D}{(P/K)^{2/3}} \gg 1 \tag{2}$$

It seems natural due to (2) to avoid the last two arguments in (1), so the following law is obtained

$$S = Const(\frac{P}{K})^{2/3} \tag{3}$$

where the $Const$ in fact depends on the Poisson ratio. This is a typical example of a scaling, power-type law. It was quite satisfactorily confirmed by experiments.

2.2 Next examples. Complete and incomplete similarity. The renormalization group

The next example will show us that the idyllic situation of the conical crack was a rare exception. Consider an infinite elastic wedge equally loaded on its sides by two identical systems of forces $p(r)$, distributed over small regions of radius r_0, and statically equivalent to couples with moment $M/2$. It is known that for plane elasticity the solution is reduced to the determining of the biharmonic Airy stress-function ψ through which the whole elastic field can be simply determined. The Airy function depends, in addition to the quantities M, r_0 on the polar coordinates r, θ and the wedge opening angle of α. So, the dimensional analysis gives

$$\psi = M\Phi(\frac{r_0}{r}, \theta, \alpha) \tag{4}$$

We will consider the elastic field at the distances r much larger than r_0, so that $r_0/r \ll 1$. Following the logic of the previous example we can neglect the argument r_0/r in (4). That means that an elastic wedge is considered as loaded by a couple in its apex. Substituting the resulting relation into biharmonic equation which the Airy function is supposed to satisfy and using the appropriate boundary conditions, we can obtain the solution in the simple form

$$\psi = \frac{M(2\theta\cos 2\alpha - \sin 2\theta)}{2(\sin 2\alpha - 2\alpha\cos 2\alpha)} \tag{5}$$

This solution was obtained by S.D. Carothers (1912) and C.E. Inglis (1922). E. Sternberg and W.T. Koiter (1958) noticed that this solution has a seemingly strange property: when α, the wedge opening angle tends to $\alpha_* \simeq 0.715\pi$, the root of denominator of (5), admissible from the physical viewpoint, the stresses at all ponts of the wedge according to (5) tend to infinity. The problem is linear, and the solution can be obtained and investigated effectively also for finite r_0. Sternberg and Koiter (1958) solved this problem by the method of integral transforms, and the results obtained turned out to be instructive.

Indeed, solving this problem we are interested exactly as in the first example not in the limit of the solution at r/r_0, but in its 'intermediate asymptotics' for

$$\frac{r_0}{r} \ll 1, \ \frac{R}{r} \gg 1 \tag{6}$$

where R is some external length-scale of the wedge. However, this intermediate asymptotics appeared to be entirely different for $\alpha < \alpha_*, \alpha > \alpha_*$ and $\alpha = \alpha_*$. As Sternberg and Koiter calculations showed, the basic term of it is like (5) for $\alpha < \alpha_*$, like

$$\psi = \frac{\bar{p}(\lambda)\Phi_1(\alpha, \theta)}{r^\lambda}, \ \bar{p}(\lambda) = \int_0^{r_0} p(r) r^{\lambda+1} dr \tag{7}$$

for $\alpha > \alpha_*$, where the function $\lambda(\alpha)$ decreases monotonically from $\lambda = 0$ at $\alpha = \alpha_*$ to $\lambda = -1/2$ at $\alpha = \pi$, and

$$\psi = M[g(r_0) - ln\frac{r}{r_0}]\Phi(\theta),\ g(r_0) = \frac{2}{M}\int_0^{r_0} p(r)r\ ln\frac{r}{r_0}dr \qquad (8)$$

We emphasize that this is a rigorous result. The relationship for $\bar{p}(\lambda)$ can be transformed to $\bar{p}(\lambda) = ConstMr_0^{\lambda}$, where $Const$ is dimensionless, whence the function Φ in (4) has a scaling power-type asymptotics for small values of the first argument

$$\Phi = (\frac{r_0}{r})^{\lambda}\Phi_1(\alpha, \theta) \qquad (9)$$

Thus, for $\alpha > \alpha_*$ the parameter r_0 cannot be removed from the governing parameters as it was for $\alpha < \alpha_*$. At the same time the asymptotics of the Airy function is determined not by the moment M, but by the combination Mr_0^{λ}, where the degree λ cannot be obtained from simple dimensional considerations. For $\alpha = \alpha_*$ the parameters M and r_0 enter the asymptotics separately. In the cases like conical crack or the wedge at $\alpha < \alpha_*$ we say that there is a *complete similarity* in the parameter r_o/r. It means also that the asymptotics we are interested in are invariant with respect to additional transformation groups correspondingly,

$$S' = S, P' = P, d' = Ad; \psi' = \psi, M' = M, r_0' = Ar_0, \qquad (10)$$

where $1 > A > 0$ is the group parameter. For the wedge with the opening angle $\alpha > \alpha_*$ the group is more complicated:

$$\psi' = A^{\lambda}\psi, M' = M, r_0' = Ar_0 \qquad (11)$$

This is a simple example of *renormalization group*, a concept very popular now in theoretical physics. We say that there is an *incomplete similarity* in the parameter r_0/r. For $\alpha = \alpha_*$ there is no similarity.

Another example of the same kind is a geometric one. Consider a smooth curve, like anormal circle. We inscribe a regular $n-$gon with the side length of η in it. For the length of the perimeter L_η

of the polygon we obtain from dimensional analysis

$$L_\eta = D\Phi(\eta/D) \tag{12}$$

where D is the diameter of the curve. For sufficiently small η/D the function Ψ is arbitrarily close to its limit, equal to π for the circle, so, asymptotically $L_\eta = \pi D$. It is clear that this asymptotics is invariant with respect to a transformation group $L_\eta^{'} = L_\eta, D^{'} = D, \eta^{'} = A\eta$. It is another example of complete similarity. As an example of incomplete similarity we consider the Mandelbrot fractal, for instance von Koch curve. The asymptotics of the function Φ in (12) for such a curve is at small η/D like $\Phi \sim C(\eta/D)^{-\alpha}$, where $\alpha = Const, 0 < \alpha < 1$, so that for L_η a scaling, power-law holds: $L_\eta = ConstD^{1+\alpha}/\eta^\alpha$. This asymptotics is invariant with respect to a simple renormalization group $L_\eta^{'} = A^{-\alpha}L_\eta, D^{'} = D, \eta^{'} = A\eta$.

3 Micromechanics

According to the micromechanical approach the properties of the material microstructure directly or indirectly observable, are explicitly introduced into consideration. The equations of macroscopic motions and those of kinetics of microstructural transformation are considered simultaneously. Thus, in our understanding, the micromechanics is the branch of mechanics studying the phenomena for which the variations of the microstructure are of governing influence for macroscopic behaviour of bodies.

If the time scales of the processes under consideration are such that the variations of the microstructure can be considered either as instantaneous, or as negligible ones, we return to the classical approach of continuum mechanics.

I would like to mention here three persons who performed the milestone works in micromechanics in the sense just mentioned. These persons are generally accepted as outstanding members of the mechanical community, and it is specially important because the mechanical community in general is rather conservative - in

the good sense of the word - in what concerns the subject of the mechanical research. Therefore the example of the outstanding people within - non outside - the mechanical community is specially important. To be modern in mechanics researchers should know micromechanics, and apply its methods. I would like to mentioned here Th.von Kármán who launched 'Aerothermochemistry',a branch of fluid mechanics concerning the fluid motions with chemical transformations and heat generation. I want to mention G.K. Batchelor (1976) who launched 'Microhydrodynamics' and considered the fundamentals of the motion of small bodies in fluids which became later the basis of modern hydrodynamics of suspensions. I mention here B. Budiansky (1981, 1986) who outlined the general approach of micromechanics of deformable solids in the papers entitled 'Micromechanics'. I am pleased to present here a citation from his second paper. It is very appropriate: 'Micromechanics is the currently fashionable designation of what is really an old subject, but one that is receiving increasing attention from theoreticians in applied mechanics. Armed with their repertoire of analytical tools, they try to relate the overall deformation and strength properties of the materials to the behaviours and interactions of their microscopic constituents.'

The natural question arises whether the coining of a new term is justified, legitimizing a new branch of continuum mechanics, and so giving it a status of certain independence? I give a positive answer to this question. The examples of the theory of oscillations, considering oscillations in a way irrelevant to their physical nature, functional analysis, cybernetics, to a lesser extent cynergetics confirm it. A general approach appears as well as unified style of the analysis of new phenomena, to a certain extent new general ideology. Seemingly uncoordinated results appear in a unified form. The transfer of results from one subject to another becomes possible as well as prediction of results based on previous experience. Therefore the legitimization of micromechanics to a unified new branch of continuum mechanics seems to be well deserved and expedient.

I will mention here a seemingly special problem of micromechanics of solids, which seems to me a characteristic and funda-

mental one for this subject. In aerothermochemistry such a problem is obviously the problem of flame propagation in combustible gas: a steady state regime of propagation of the chemical reaction zone, accompanied with the heat generation, heat conduction and diffusion. In micromechanics of solids such a problem is the mathematically similar problem of neck propagation in polymers (Barenblatt 1974a, b). This phenomenon, discovered by chemists in the early 30s was immediately noticed by A. Nadai as fundamentally important. The 'neck' - steady state fast deformation zone - propagation is accompanied with the transformation of the material microstructure, specific stress induced diffusion and heat generation.

4 Application of scaling approach to the kinetics of fatigue crack propagation

A classical result in fatigue fracture is the well-known scaling law by Paris and Erdogan (1963) for the velocity of the crack propagation in multi-cycle fatigue

$$\frac{dl}{dn} = A(\Delta K)^m \tag{13}$$

Here dl/dn is the fatigue crack velocity per cycle averaged over the cycle, ΔK is the stress intensity factor amplitude. The quantities A and m are usually considered as universal constants for a given material. To analyse that let us consider the kinetic diagram (13) from the viewpoint of the similarity approach (Barenblatt & Botvina, 1981, 1983). The average velocity dl/dn can depend in principle upon the following quantities: $\Delta K = K_{\max} - K_{\min}, R = K_{\min}/K_{\max}$ - asymmetry of the loading ($K_{\max}, K_{\min}$ are correspondingly maximal and minimal stress intensity factors over the cycle), h - characteristic specimen size, f-frequency, K_{IC} - fracture toughness, a standard characteristic of strength, σ_y- the yield stress, t-time.

The dimensional analysis gives

$$\frac{dl}{dn} = \left(\frac{\Delta K}{\sigma_Y}\right)^2 \Phi\left(\frac{\Delta K}{K_{IC}}, R, z, ft\right) \tag{14}$$

where

$$z = \frac{\sigma_Y \sqrt{h}}{K_{IC}} \tag{15}$$

is the basic similarity parameter. An asymptotic stage is considered, where the influence of the argument ft disappears. Intermediate asymptotic character of the fatigue crack extension is clearly confirmed by the analysis of the fracture surface: a regular system of striations appears at this stage. Moreover, the argument $\Delta K/K_{IC}$ is small, and we want to consider asymptotic relations. Then, two possibilities appear: complete similarity when the limit of Φ at $\Delta K/K_{IC} \to 0$ is finite or not. If it is finite, we would obtain the scaling law (13) with $m = 2$, which is practically never the case, except of some aluminium alloys. Let us assume that the incomplete similarity in the parameter $\Delta K/K_{IC}$ takes place at the intermediate stage of the fatigue crack extension:

$$\Phi = (\frac{\Delta K}{K_{IC}})^{\alpha} \Phi_1(R, z); \quad \frac{dl}{dn} = \frac{(\Delta K)^{2+\alpha}}{\sigma_Y^2 K_{IC}^{\alpha}} \Phi_1(R, z) \tag{16}$$

It means that the scaling law (13) is valid, but the quantities A and $m = \alpha + 2$ depend on the basic similarity parameter z. That means that they depend not only upon the material properties, but also upon the specimen size. The processing of the experimental data showed that this dependence could be very strong (Figure 2), so that the designers should be careful in using the results of the standard fatigue experiments with small specimens for predicting the life-time of large structures.

An important note. In the middle of kinetic diagram the mechanism of fracture starts to change: the traces of static fatigue modes, such as dimples appear on the fracture surface. It is connected quantitatively with reaching a certain critical stress-intensity factor K_{GY} equal by order of magnitude to $\sigma_Y \sqrt{d}$, where d is the microstructural length-size. Therefore, plausibly, the Paris-

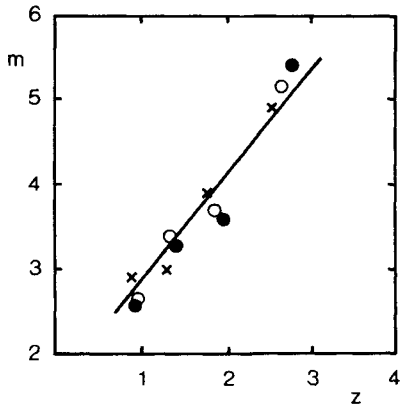

Fig. 2 The dependence of the exponent in the Paris-Erdogan scaling law (13) on the similarity parameter z for steel 4340 for specimens of various orientation with respect to the rolling direction (Barenblatt, Botvina (1981), processing of data of F.A. Heiser and W. Mortimer)

Erdogan kinetic curve consists of two pieces corresponding to $\Delta K \gg K_{GY}$ and $\Delta K \ll K_{GY}$. Apparently it was not properly identified because the values of m, corresponding to two branches of kinetic curve were sufficiently close.

5 Self-similar, self-oscillation regime of fatigue crack extension

5.1 Forsyth effect

Sometimes the kinetic diagrams are not single-valued curves and there exists a rather large overlapping range on these curves. Fracture surface analysis shows that upper and lower branches of non-single-valued kinetic curves correspond to different micromechanisms of fracture. This phenomenon gives rise to a peculiar and practically important regime of self-oscillational and simultaneously self-similar phenomenon of fatigue crack propagation dis-

covered by P.J.E. Forsyth (1976). Forsyth performed a fatigue experiment with constant amplitude of loading on a slotted plate aluminium alloy DTD 687 specimen. On the fracture surface he observed a sequence of alternating smooth and rough strips sharply bounded by curved lines (Figure 3). Forsyth noted that in neighbouring strips different micromechanisms of fracture took place. By processing his experimental results he discovered that for both sequences of curvilinear boundaries (smooth-rough and

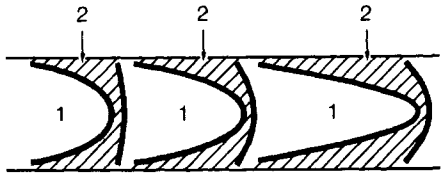

Fig. 3 Alternating parts of the fracture surface in the experiments of Forsyth (1976) (Schematic representation). 1. Smooth parts, 2. Rough parts.

rough-smooth transitions) the scaling relationship is valid

$$\frac{\sqrt{a}}{l} = const, \tag{17}$$

a being the maximum crack depth, l the crack front contour length, $Const$ is different for different sequences. Forsyth immediately understood the value of this result for the purpose of failure analysis, 'fractodiagnostics', as we call this technique now (Botvina, 1989). Since that time Forsyth's discovery has received further confirmations and practical applications (Botvina, 1989; Botvina *et al.* (1981)). Nowadays it is clear that the Forsyth effect is a manifestation of a phenomenon of fundamental importance. Therefore an attempt to understand it from the general viewpoint of fracture mechanics (Barenblatt & Botvina, 1993) seems to be expedient.

5.2 The model

The proposed model is based on two key points. The first point is the existence, at least for some aluminium and titanium alloys and certain steels, of discontinuities in the fatigue fracture kinetic diagrams. It was discovered by Shabalin (1958) and later confirmed by other authors. The second point is the formation of a self-similar intermediate asymptotic regime of scaling type: incomplete similarity.

So we assume that the kinetic diagram relating crack extension rate dl/dn (averaged over a cycle) with stress-intensity factor amplitude is a non-single-valued curve with a large overlapping range of stress-intensity-factor amplitude. The examples of such curves can be found in the book by Botvina (1989). It is essential that the upper and lower branches of this non-single-valued kinetic curve correspond to different micromechanisms of fracture. As often appears in such cases (the Van der Waals curve is a classical example) it is plausible that there exists an intermediate unstable regime of fracture. It is more convenient for us to transform the coordinate along the abscissa axis. Indeed,

$$\Delta K = K_{\max}(1 - R), \; R = K_{\min}/K_{\max} \tag{18}$$

so, bearing in mind that R is kept constant during the experiment, it is always possible to replot the kinetic curve in the form (Fig. 4)

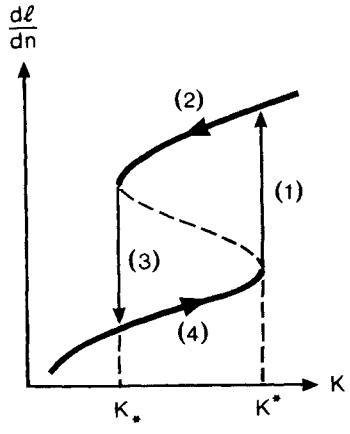

Fig. 4 Schematic kinetic diagram of fatigue fracture and proposed hysteresis regime.

$$\frac{dl}{dn} = f(K) \tag{19}$$

where K the material property - is maximal stress intensity factor, corresponding to a given crack extension rate dl/dn averaged over the cycle. We emphasize that K does not coincide with K_{IC}. Indeed, K is a variable fracture toughness which corresponds to stable crack propagation whereas K_{IC} requires for its determination the beginning of catastrophic crack extension in static loading. Two critical values of K are shown on the Figure: K^* corresponding to the highest value for the 'slow' mode of crack propagation, and K_* to the lowest value of the fast propagation mode. A plausible unstable regime is shown by a dotted line.

We emphasize first of all that the crack contour is a curvilinear one. Indeed, if it were rectilinear, the crack under constant load cannot stop after beginning its extension, because the stress intensity factor would only increase. We assume furthermore that the crack extension process follows the hysteresis loop (1) - (2) - (3) - (4) shown in the Figure, so that the transition from slow to fast regime corresponds to $K = K^*$, and the transition from fast to slow regime corresponds to $K = K_*$.

Note that the very possibility of an analytic consideration of such a complicated problem of mixed mode extension of a crack with a curvilinear contour is due to the following important fact: after the first jumps, when the crack contour length becomes significantly larger than the specimen thickness l_0 an intermediate asymptotic self-similar regime begins. During this regime each step repeats (on a different length scale) the previous one from the same sequence. Certainly, this regime can last only until the crack head closely approaches the specimen side-edge, when the terminal stage of static failure begins. Transition boundaries (the slow-fast and fast flow transition curves) correspond to transition from one branch of the kinetic diagram to another.

It is important that for the intermediate asymptotic self-similar regime, covering a major part of Forsyth's observation the double inequality

$$l_0 \ll l \ll a \tag{20}$$

is valid.

Now to the most essential point of the model construction. According to the dimensional analysis, we can write at an arbitrary point of the contour of the crack for the stress intensity factor (coefficient at the singularity at the crack contour, obtained from the solution of the corresponding elasticity problem):

$$N = \sigma_{\max}\sqrt{a}\ \phi(\frac{s}{l}, \frac{l_0}{l}) \tag{21}$$

where ϕ is a certain dimensionless function of its dimensionless arguments, s is the arc-length along the crack contour reckoned from the most advanced point of the crack contour. According to the inequality (20) the argument l_0/l is small.

Furthermore, at every point of the transition lines one of the limiting conditions

$$N = \frac{K^*}{\pi} \text{ or } N = \frac{K_*}{\pi} \tag{22}$$

should hold, according to which sequence belongs to the transition line. The scaling law (17) is valid if and only if

$$\phi(\frac{s}{l}, \frac{l_0}{l}) = Const\frac{l_0}{l}, \tag{23}$$

i.e. if there is incomplete similarity in the small argument l_0/l. The relations (21) and (23) give

$$\frac{\sqrt{a}}{l} = Const\frac{K_*}{\sigma_{\max}l_0} \text{ or } \frac{\sqrt{a}}{l} = Const\frac{K^*}{\sigma_{\max}l_0} \tag{24}$$

which are similar (but not identical) with the empirical relation proposed by Forsyth. In Forsyth's relation instead of K^* and K_* there enters K_{IC} which seems to be less appropriate.

6 Conclusion

The work is material science, and specially in disordered materials like ceramics is now of primary importance for the whole of mankind. The flavour of coming discoveries is felt in everyday work in this field, discoveries of decisive value not only for science and technology but also for everyday life. We should not miss our chance to contribute to this stream of research efforts. I am sure that advanced scaling and similarity methods presented here could be very helpful in our understanding and mathematical modelling.

References

Barenblatt, G.I. (1974a) Neck propagation in polymers. **Rheologica Acta**, 13, 924-933.

Barenblatt, G.I. (1974b) Methods of combustion theory in the deformation, fracture and flow of polymers, in **Deformation and Fracture of High Polymers** (eds H. Henning Kausch, J.A. Hassel and R.G. Jaffe) , Plenum Press, New York, pp. 91-111.

Barenblatt, G.I. and Botvina, L.R. (1981) Incomplete self-similarity of fatigue in the linear range of crack growth. **Fatigue Engng. Mater. Struct.**, 3, 193-202.

Barenblatt, G.I. and Botvina, L.R. (1983) Self-similarity of fatigue fracture. Damage Accumulation. **Bull. Acad. Sci. USSR, Mechanics of Solids**, 4, 88-92.

Barenblatt, G.I. and Botvina, L.r. (1993) Self-oscillatory modes of fatigue fracture and the formation of self-similar structures at the fracture surface. **Proc. Roy. Soc. Lond.**, A442, 489-494.

Batchelor, G.K. (1976) Development in microhydromechanics, in **Theoretical and Applied Mechanics** (ed W.T. Koiter), North-Holland, pp. 33-55.

Benbow, J.J. (1960) Cone crack in fused silica. **Proc. Phys. Soc.**, B75, 697-699.

Botvina, R. (1989) **The Kinetics of Fracture of Structural Materials**, Nauka, Moscow (in Russian).

Botvina, L.R., Limar, L.V., and Logovikov, B.S. (1981) Estimation of jump-like growth parameters of fatigue crack in compressor blades from BT3-1 titanium alloy. **Soviet Mater. Sci.**, 1, 71-74.

Budiansky, B. (1981) Micromechanics, **Computers and Structures**, 16, No. 1-4, pp. 3-12.

Budiansky, B. (1986) Micromechanics II. **Proc. 10th US National Congress of Applied Mechanics**, Austin, pp 1-8.

Carothers, S.D. (1912) Plan strain in a wedge. **Proc. Roy. Soc. Edinburgh**, 23, No. 2, 292-306.

Forsyth, P.J.E. (1976) Some observations and measurements on mixed fatigue tensile crack growth in aluminium alloys. **Scripta Metall.**, 10, 383-386.

Inglis, C.E. (1922) Some special cases of two-dimensional stress and strain. **Trans. Inst. Naval. Archit.**, 64, 253-258.

Paris, P.C. and Erdogan, F. (1963) A critical analysis of crack propagation laws. **J. Basic Engng. Trans. ASME**, Sec. D, 85, 528-534.

Shabalin, V.I. (1958) On discontinuity in fatigue curves of duraluminium. **Doklady Ac. Sci. USSR**, 122, 600-604.

Sternberg, E. and Koiter, W.T. (1958) The wedge under a concentrated couple: a paradox in the two-dimensional theory of elasticity. **J. Appl. Mech.**, 25, No. 4, 575-581.

von Kármán, Th. (1963) Aerothermochemistry, in **From Low Speed Aerodynamics to Astronautics** (Th. von Kármán), Pergamon Press, Oxford, pp. 29-46.

PART ONE
FRACTURE MECHANICS OF CONCRETE

Chair: P. Rossi

2 MULTIFRACTAL NATURE OF MATERIAL MICROSTRUCTURE AND SIZE EFFECTS ON NOMINAL TENSILE STRENGTH

A. CARPINTERI, B. CHIAIA and G. FERRO
Department of Structural Engineering, Politecnico di Torino, Turin, Italy

Abstract

Damage, strain localization, and fracture are not always interpretable in the framework of continuum mechanics. In particular, the scale effect on nominal tensile strength has not found satisfactory explanations. The reason for this has to be sought in the fact that the micromechanical damage phenomena, and thus the inherent disorder of the material, have been disregarded. Fractal geometry and renormalization group theory can provide today a rational and consistent explanation, harmonizing and enriching the empirical approach of Weibull and the phenomenological assumption of Griffith. Material ligaments at peak stress can be considered as multifractals, of dimension 1.5 at small scales, and dimension 2 at large scales. This means that, at large scales, the disorder is not visible, the size of the heterogeneities being limited. A transition from extreme disorder (slope $-1/2$) to extreme order (zero slope) may therefore be evidenced in the bilogarithmic strength versus size diagram. A Multifractal Scaling Law (MFSL) is proposed with a concavity opposite to that of the Bažant's Size Effect Law (SEL). The size effects on some significant experimental tests reported in the literature are interpreted by the MFSL very consistently.

1 Introduction

Several physical phenomena can be analyzed through continuum mechanics, whenever only one length or energy scale is relevant, namely the macroscopic scale. On the other hand, it is generally true that, where a critical phenomenon (e.g., material failure) is imminent, also other length or energy scales become relevant together with the macroscopic one: they represent those microscopic or mesoscopic phenomena that are interacting and concurring to produce the macroscopic phenomenon. Continuum mechanics has been the basis for structural mechanics for more than a century. Only recently has it emerged that damage, strain localization, and fracture phenomena are not always interpretable in the framework of continuum mechanics. In particular, the scale effects on nominal tensile strength have not found satisfactory explanations (Carpinteri, 1986). The reason for this has to be sought in the fact that the micromechanical damage phenomena, and thus the inherent disorder of the material, have been disregarded. A dramatic dichotomy is

Fracture of Brittle Disordered Materials: Concrete, Rock and Ceramics. Edited by G. Baker and B.L. Karihaloo. Published in 1995 by Taylor & Francis, 2 Park Square, Milton Park, Abingdon, Oxon, OX14 4RN. ISBN: 0 419 19050 3.

still present between, on the one hand, structural engineers, who pay close attention to macroscopic phenomena and whose models present an excessive regularity, and, on the other, material scientists, who devote greater attention to microscopic phenomena and whose models present an excessively local character.

The present paper represents an attempt to break down these barriers by adopting approaches that are completely new for solid mechanics, i.e., fractal geometry (Mandelbrot, 1982; Falconer,1990) and renormalization group theory (Wilson, 1971, 1979; Barenblatt, 1979; Herrmann and Roux, 1990). This is the only way to provide a rational and consistent explanation of the size effects on tensile strength of disordered materials.

2 Fractal nature of material ligament at maximum load

It is well-known that the nominal tensile strength of many materials undergoes very clear size effects. The usual trend is that of a strength decrease with size, and this is more evident for disordered (i.e., macroscopically heterogeneous and/or damaged) materials. Griffith (1921) explained the strength size effect in the case of glass filaments, assuming the existence of inherent microcracks of a size proportional to the filament cross-sectional diameter. Some years later Weibull (1939) gave a purely statistical explanation to the same phenomenon according to the weakest-link-in-a-chain concept. Only recently have the two views been harmonized, enriching the empirical approach of Weibull with the phenomenological assumption of Griffith (Freudenthal, 1968; Jayatilaka, 1979; Carpinteri, 1989). A *statistical size distribution of self-similarity* may be defined (Carpinteri, 1986, 1989) for which the most dangerous defect proves to be of a size proportional to the structural size. This corresponds to materials presenting a considerable dispersion in the statistical microcrack size distribution (disordered materials). In this case, the power of the LEFM stress singularity, 1/2, turns out to be the slope of the strength versus size decrease in a bilogarithmic diagram. When the statistical dispersion is relatively low (ordered materials) the slope is less than 1/2 and tends to zero for regular distributions (perfectly ordered materials).

Although the above-described view contains the fractal concept of self-similarity, this is circumscribed only to the defect of maximum size, whereas the disordered nature of the material microstructure is completely disregarded. The real nature of the material will be herein described using a more complex fractal model, where the property of self-similarity is extended to the whole defect population. On the other hand, slope values higher than 1/2 would represent, with both models, a degree of disorder that is so high as to be usually absent in real materials.

Let us assume that the reacting section or ligament of a disordered material at peak stress could be represented as a fractal space of dimension $\alpha = 2 - d_\sigma$, with $1 < \alpha \leq 2$ and, therefore, $0 \leq d_\sigma < 1$. The dimensional decrement d_σ may be due to the presence of cracks and voids and hence, generally, to a cross-sectional weakening. A typical fractal set - the *middle-third Cantor set* - is shown in Fig.1.

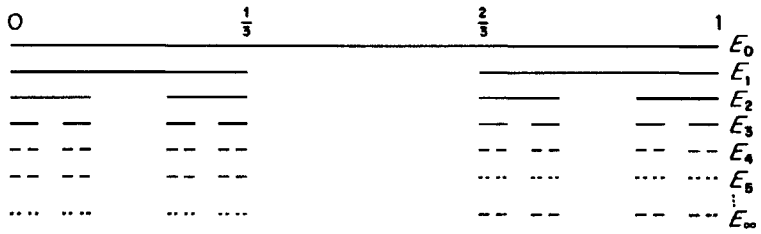

Fig. 1. Fractal nature of material ligament.

This set may be constructed from a unit interval by a sequence of self-similarity deletion operations. It can be demonstrated that the fractal dimension of the set is 0.631, and therefore that it can be measured consistently only as a length raised to 0.631. Let us consider two bodies, geometrically similar and made up of the same disordered material (Fig. 2). If the ratio of geometrical similitude is equal to d and the *renormalized tensile strength* σ_N^* is assumed to be a material constant and to have the physical dimensions [force]x[length]$^{-(2-d_\sigma)}$, we have (Carpinteri, 1992)

$$\sigma_N^* = \frac{F_1}{1^{2-d_\sigma}} = \frac{F_2}{d^{2-d_\sigma}} \tag{1}$$

F_1 and F_2 being the ultimate tensile forces acting on the two bodies respectively.

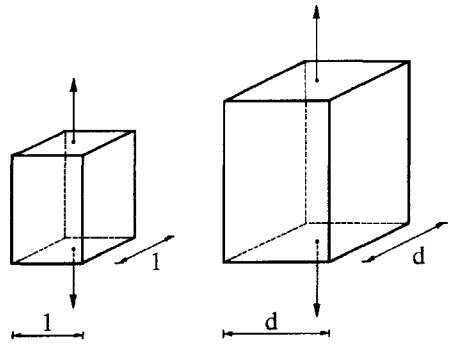

Fig. 2. Size-scaled bodies.

On the other hand, the apparent nominal tensile strengths are respectively

$$\sigma_N^{(1)} = \frac{F_1}{1^2} \tag{2}$$

$$\sigma_N^{(2)} = \frac{F_2}{d^2} \tag{3}$$

where the latter, according to eq. (1), becomes

$$\sigma_N^{(2)} = \sigma_N^{(1)} d^{-d_\sigma} \tag{4}$$

We can write the relationship between nominal strengths related to different sizes in logarithmic form

$$\log \sigma_N = \log \sigma_N(1) - d_\sigma \log d \tag{5}$$

Eq. (5) represents a straight line with slope $-d_\sigma$ in the $\log \sigma_N$ versus $\log d$ plane (Fig. 3).

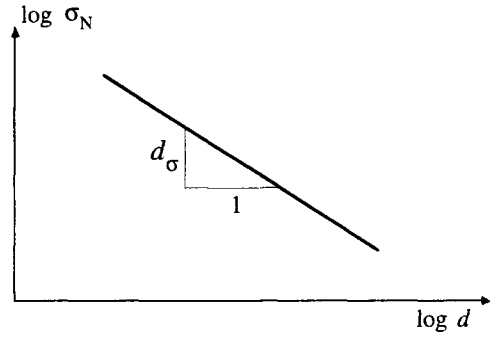

Fig. 3. Size-scale effect on tensile strength.

An alternative way to explain the decrease of the nominal tensile strength with specimen size is that of considering a sequence of scales of observation. If the total force F transmitted to the specimen is invariant with respect to the scale of observation, we have

$$F = \sigma_1 A_1 = \sigma_2 A_2 = ... = \sigma_{n-1} A_{n-1} = \sigma_n A_n = \sigma_{n+1} A_{n+1} = ... = \sigma_\infty A_\infty \tag{6}$$

where the first scale of observation could be the macroscopic one, with $\sigma_1 A_1 = \sigma_N A$, A being the cross-sectional area, and the asymptotic scale of observation could be the microscopic one, with $\sigma_\infty A_\infty = \sigma_N^* A^*$, A^* being the measure of the fractal set representing the damaged ligament.

From the equality between the extreme members of eq.(6) we get

$$\sigma_N = \sigma_N^* \left(\frac{A^*}{A} \right) \tag{7}$$

and therefore

$$\sigma_N = \sigma_N^* \left(\frac{d^{2-d_\sigma}}{d^2} \right) \tag{8}$$

with d equal to the characteristic dimension of the cross section. From eq.(8) we can get a generalization of eq.(5)

$$\log \sigma_N = \log \sigma_N^* - d_\sigma \log d \tag{9}$$

Renormalization group relations analogous to eq. (9) have been proposed by Wilson (1971, 1979) in quantum field theory and statistical mechanics, as well as by Barenblatt (1979) in the intermediate asymptotics description of turbulence and blasting.

3 Multifractal Scaling Law

For size scales tending to infinity, or, in other words, for very large specimens, tensile strength σ_N may appear constant by varying the specimen size (Tang et al., 1992; Kim and Eo, 1990), whereas, for size scales where random self-similarity holds, the so-called "universal property" of the system (σ_N^*) is constant, although it is represented by a physical quantity with unusual dimensions. The last result represents the target of the so-called "renormalization" procedure (Wilson, 1971, 1979), i.e., the determination of physical quantities that are invariant under a change of length scale.

In physical reality, material ligaments at peak stress can be considered as *multifractals* (Mandelbrot, 1982; Falconer, 1990), of dimension 1.5 at small scales, and dimension 2 at large scales. This means that, at large scales, the disorder is not visible, the size of the heterogeneities being limited. A transition from extreme disorder (slope $-1/2$) to extreme order (zero slope) may therefore be evidenced in the diagram $\log \sigma_N$ versus $\log d$ (Fig 4). Probably, for even smaller scales, a chaotic disorder could prevail over the maximum fractal disorder with slope $-1/2$.

The asymptotic trends of tensile strength can be described also in the corresponding proportional diagram as in Fig. 5. For size scale tending to zero, tensile strength tends to infinity and renormalization group theory, already applied in other branches of science, is able to provide a definitive explanation of the size effects on strength. On the other hand, we should recall the first attempt by Griffith (1921) to give some rational explanation to the strength increase by decreasing the cross-sectional area of glass filaments.

The analytical expression of the Multifractal Scaling Law (MFSL) is the following (Fig. 5):

$$\sigma_N = \left(A + \frac{B}{d} \right)^{\frac{1}{2}} \tag{10}$$

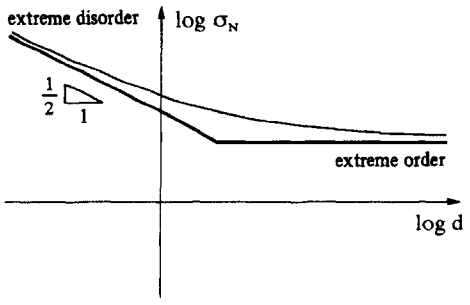

Fig. 4. Multifractal Scaling Law (bilogarithmic diagram).

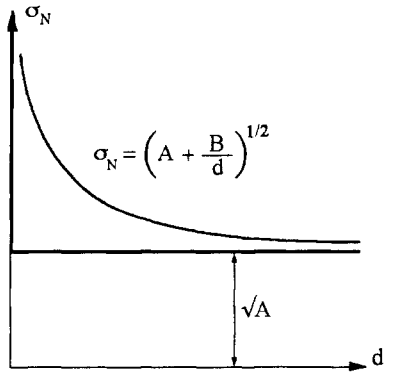

Fig. 5. Multifractal Scaling Law (proportional diagram).

where:

σ_N = nominal tensile strength;

d = characteristic structural size;

$A = [[F][L]^{-2}]^2$ = constant with physical dimensions equal to the square of a stress;

$B = [[F][L]^{-\frac{3}{2}}]^2$ = constant with physical dimensions equal to the square of a stress-intensity factor.

The two constants will be determined in each case by means of a non-linear least-squares numerical algorithm, such as the Levenberg-Marquardt method (1963), in order to perform the best-fitting of the experimental data. The physical requirements previously exposed are thus respected

$$\lim_{d \to \infty} \left(A + \frac{B}{d}\right)^{\frac{1}{2}} = \sqrt{A} \tag{11}$$

$$\lim_{d\to 0^+}\left(A+\frac{B}{d}\right)^{\frac{1}{2}}=+\infty \tag{12}$$

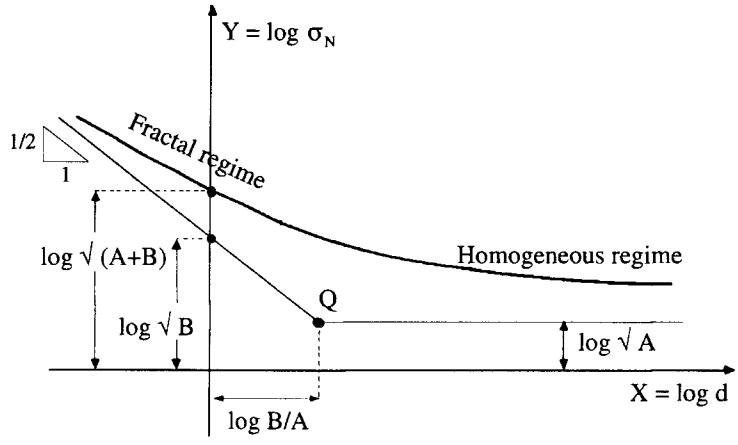

Fig. 6. Physical meaning of the parameters A and B.

In the bilogarithmic diagram shown in Fig. 6 ($X = \log d; Y = \log \sigma_N$), the analytical expression becomes

$$Y(X)=\frac{1}{2}\log\left(A+\frac{B}{10^X}\right) \tag{13}$$

The asymptotes in the bilogarithmic plot present peculiar physical meanings (Fig. 6). The horizontal asymptote, corresponding to the large sizes (*homogeneous* regime), has the following expression:

$$H_1(X)=\log\sqrt{A} \tag{14}$$

while the oblique asymptote, which corresponds to the macroscopic dimension d tending to zero (i.e., $X \to -\infty$) and governs the *disordered* or *fractal* regime, has the following expression:

$$H_2(X)=-\frac{1}{2}X+\log\sqrt{B} \tag{15}$$

We wish to emphasize the fundamental difference with respect to Bažant's Size Effect Law (SEL), where the underlying physical arguments are conceptually the opposite. In that case, in fact, a constant asymptotic value of strength is reached for sizes tending to zero, where Limit Analysis is supposed to govern the failure mechanism, whereas, in the MFSL, Limit Analysis comes into play only in correspondence with the *homogeneous* regime, when the disordered microstructure has been homogeneized at the larger scales.

On the other hand, according to the MFSL, Linear Elastic Fracture Mechanics is supposed to govern the collapse mechanism of an unnotched material as the characteristic flaw size a becomes comparable to the macroscopic dimensions or, that is the same, as the disorder comes essentially into play. Thus, as the structural size progressively decreases, the behavior (Fig. 6) tends to the oblique asymptote (*disordered* or *fractal* regime) which is controlled by the parameter B, whose dimensions are, significantly, those of a stress-intensity factor raised to square. Furthermore, as the structural size d tends to zero, the slope of the bilogarithmic diagram tends to -0.5, which is the LEFM scale effect simply provided by Dimensional Analysis (Carpinteri, 1982). The Griffith's mode of collapse, governed by a 0.5 stress singularity, becomes the main failure mechanism only in the limit of macroscopic size d tending to zero. From this point of view, the MFSL represents an ideal prosecution of Griffith's pioneering work (1921), where the glass fiber's strength was found to be surprisingly high if compared with that of normal sized glass specimens.

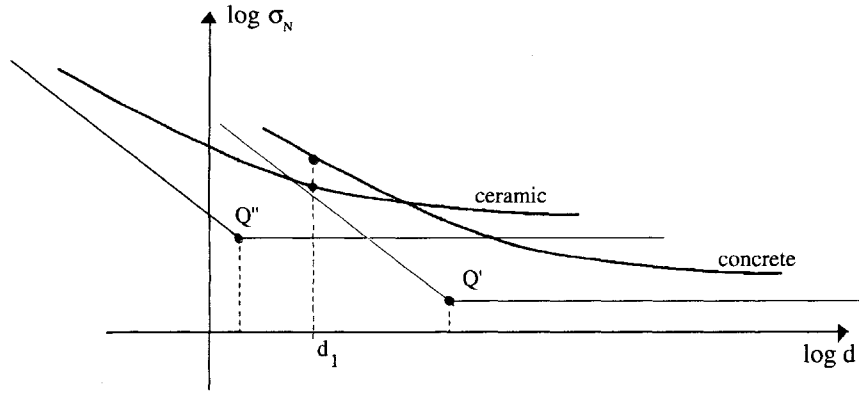

Fig. 7. Multifractal Scaling Law for two different material microstructures.

The intersection points are indicated in Fig. 6. Point Q is the intersection of the two asymptotes, and its horizontal coordinate is given by

$$X_Q = \log \frac{B}{A} \tag{16}$$

where the dimension of the quantity B/A is that of a length. Point Q ideally separates the disordered regime from the ordered (homogeneous) regime. It seems to be natural to associate this quantity with the microstructural characteristic size l, which could be, in the case of concrete, proportional to the maximum aggregate size d_{max}

$$l = \frac{B}{A} = \alpha d_{max} \tag{17}$$

It is reasonable to suppose that, for fine grained materials (rocks, ceramics, metals) this value should be considerably smaller than in the case of concrete, thus providing the MFSL to shift horizontally to the left in the bilogarithmic diagram. Given a particular size d_1, for example, a concrete specimen could behave according to the fractal disordered regime, whereas a ceramic or glass specimen of the same size could be set in the (nearly) horizontal branch (Fig. 7).

The ranges of pronounced scale effects, corresponding to the fractal regime, have then to be individuated case by case for each material and, more precisely, for each microstructure. This explains why, in materials such as metals, the strength size effect is not observed, in the absence of initial cracks, at the usual structural dimensions. In order to clarify the physical meaning of the various terms, eq. (10) may be rearranged in the form

$$\sigma_N = f_t' \left(1 + \frac{\alpha d_{max}}{d}\right)^{\frac{1}{2}} \tag{18}$$

where the non-dimensional term in the brackets represents the positive deviation, due to disorder, from a limit nominal strength f_t', valid for infinitely large sizes. In this case α and f_t' represent the two constant parameters to be determined by the best-fitting of the experimental data.

4 Experimental confirmation

The Multifractal Scaling Law, proposed in the previous section, will now be used to analize the size effect on some significant experimental tests reported in the literature. The experimental results concern tests on four different unnotched specimen geometries. In addition, the Bažant's Size Effect Law (SEL) will be compared with the MFSL. The SEL, obtained from the hypothesis that a notch of length proportional to the specimen size exists, not always gives reliable results. Furthermore, the validity of that hypotesis may be questionable.

The first geometry that will be discussed is that of a four-point bending test carried out by Sabnis and Mirza (1979) for unnotched specimens. A number of plain model concrete beams with rectangular section were cast from the same mix (0.7:1:3.6), using sand passing sieve No.8, and they were then cured identically. These specimens ranged from 6 mm x 9 mm to 100 mm x 150 mm in cross section sizes. Each beam presented a span of four times its depth. The loading supports were accomplished with steel plates and rollers which were modelled to the same scale as the test beams. Conventional bending theory was used to calculate the extreme-fiber stress.

The test results (average values) are plotted as circular data points in a $\log \sigma_N$ versus $\log d$ diagram (Fig. 8). The MFSL in the form of eq.(10) was fitted using a standard computer library subroutine based on the Levenberg-Marquardt algorithm. In this way we obtain the MFSL as the regression curve. The val-

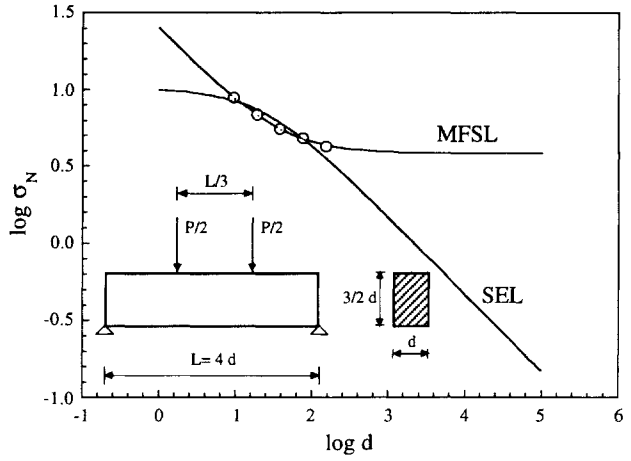

Fig. 8. Multifractal Scaling Law against Size Effect Law (Sabnis and Mirza, 1979).

ues of the parameters A and B are the following: $A = 14.668$ MPa^2 and $B = 616.31$ MPa^{2}mm. The square root of the parameter A represents the asymptotic value of the nominal strength for $d \to \infty$. In this case we obtain $f_t' = \sqrt{A} = 3.830$ MPa while the parameter $l = B/A = 42.02$ mm could represent a characteristic size for the microstructure.

The correlation coefficient R is equal to 1.000 for MFSL and to 0.952 for SEL. This means that the MFSL gives an excellent fitting for the test data. Moreover, graphically it is evident how the data in the $\log \sigma_N$ versus $\log d$ plane suggest a curvature opposite to that of SEL and that, increasing the structural size d, the decrement of the nominal strength tends to attenuate. This means that, for $d \to \infty$, the nominal strength should have an horizontal asymptote, as predicted by the MFSL.

The second geometry that we consider is a splitting cylinder test by Hasegawa, Shioya and Okada (1985). The size range of these tests was 1:30. All the specimens had the thickness of 500 mm and the maximum aggregate size of concrete was 25 mm. The average compressive strength of the 100 mm diameter and 200 mm height cylinders, was 23.4 MPa. The values of the MFSL constants are the following: $A = 2.09$ MPa^2 and $B = 416.3$ MPa^{2}mm. The horizontal asymptote for $d \to \infty$ is given by $f_t' = \sqrt{A} = 1.45$ MPa, while the characteristic size is $l = B/A = 199.2$ mm. The ratio between l and the maximum aggregate size is $l/d_{max} = 7.69$. The fitting of the test data with the MFSL gives a correlation coefficient R=0.966 while from SEL we obtain a value R=0.663. The fitting is performed by considering the strength values averaged for the same size. It is important to note how in this case the SEL not only presents a worste fitting but also indicates a trend that is completely different from the experimental one (Fig. 9).

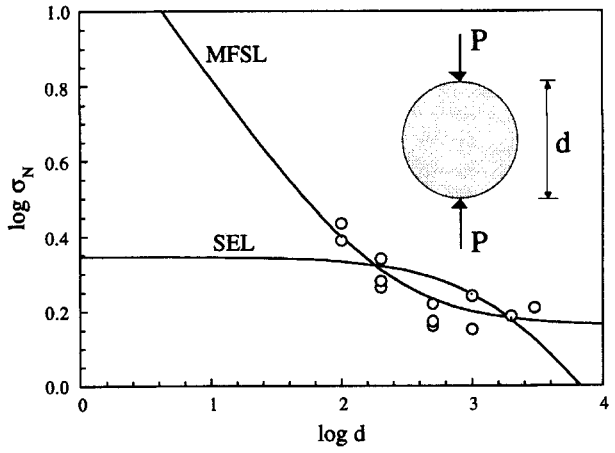

Fig. 9. Multifractal Scaling Law against Size Effect Law (Hasegawa et al., 1985).

The third geometry regards the pull-out tests performed by Eligehausen, Bouška, Červenka and Pukl (1992). Specimens and headed anchor bolts with three different sizes and the same geometrical shape were used. For corresponding dimensions the scaling ratio 1:3:9 was applied, the actual embedment length being 50, 150 and 450 mm, respectively. All the specimens were made of concrete of nominally identical quality with a specified cube strength $f'_c = 30$ MPa while the tensile strength, measured by splitting test, was $f'_t = 3.0$ MPa. The water-cement ratio was 0.58 and the maximum aggregate size of 22 mm. The tensile force was transferred to the anchor through a shaft with two spherical hinges to minimize bending moments. In all tests failure was caused by pulling out a concrete cone. The shape of this cone was approximately similar for all embedment depths.

Applying the MFSL and fitting the strength average values (Fig.10), the parameters A=0.269 MPa^2 and B=117.98 MPa^{2}mm are obtained. The strength for $d \to \infty$ proves to be $f'_t = \sqrt{A} = 0.518$ MPa while the characteristic size $l = B/A$ is 438.6 mm. The value of the nondimensional quantity l/d_{max} is equal to 19.9. The comparison between the correlation coefficients R, equal to 0.996 for MFSL and to 0.977 for SEL, allows us to affirm that, even in this case, the MFSL fits the experimental data better than the SEL.

The last geometry that will be presented is that of a torsional test of reinforced concrete beams realized by Bažant, Sener and Prat (1988). The test specimens were square prisms of cross-section side d and length L. Three specimen sizes characterized by d=38.1, 76.2 and 152.4 mm were used, and the ratio L/d=8/3 was the same for all beams. The beams were loaded in torsion by opposite couples at their ends. The arms of the loading couples at the beam ends were 19.1, 38.2 and 127 mm. The forces of the couples were applied at distance a from the beam end, such that a/L=3/32 for all beams. The specimens were made of microconcrete

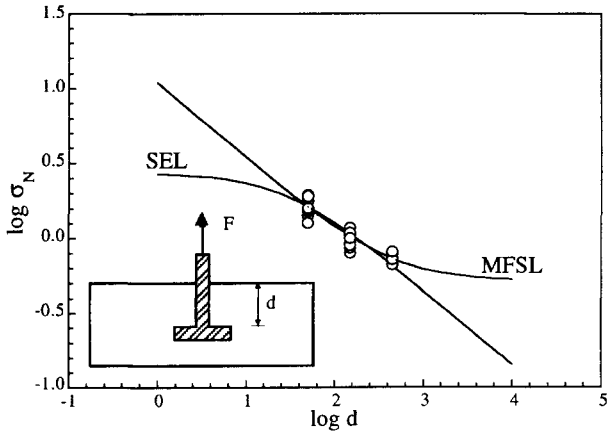

Fig. 10. Multifractal Scaling Law against Size Effect Law (Eligehausen et al., 1992).

with maximum gravel size 4.8 mm and maximum sand size 3.35 mm. The mix ratio (cement:sand:gravel:water) was 1:2:2:0.6. Three companion cylinders of diameter 76.2 mm and length 152.4 mm were also cast from each batch. The uniaxial compression strength of these cylinders was f'_c= 43.6 ÷ 44.1 MPa. The reinforced specimens of the aforementioned three sizes contained four longitudinal bars placed in the cross-section corners with a cover of 8.1, 16.3 and 31.5 mm, respectively. Deformed bars of diameters 3.18, 6.35 and 12.7 mm were used. For the smallest diameters, the yield strength was f_y=310 MPa and for the largest ones it was f_y=413 MPa.

The parameters A and B of the MFSL in this case are equal to 1.869 MPa^2 and to 494.52 MPa^{2}mm, respectively. The asymptotic strength for $d \to \infty$ results $\tau'_N = \sqrt{A}$ = 1.367 MPa, while the characteristic size, B/A, is l = 246.6 mm with the ratio l/d_{max} equal to 55.11. The fitting was performed for both laws on the average strength values. In this case the MFSL goes exactly through all the experimental data giving a correlation coefficient equal to 1.000. On the other hand, for the SEL the value R=0.979 is obtained. From Fig. 11 it is possible to observe how the two laws have a similar trend only in the range of the experimental data.

Acknowledgements

The present research was carried out with the financial support of the Ministry of University and Scientific Research (MURST) and the National Research Council (CNR).

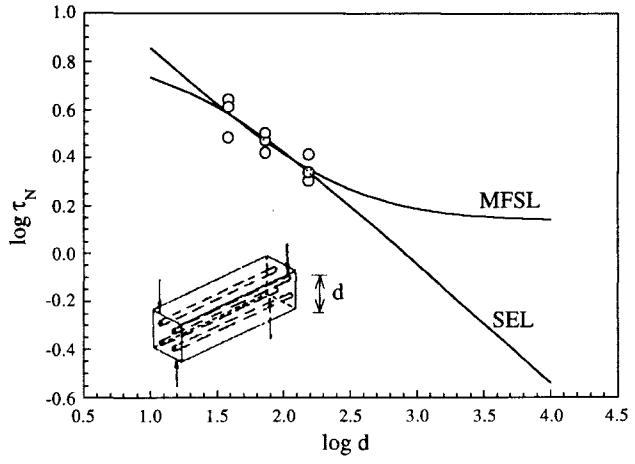

Fig. 11. Multifractal Scaling Law against Size Effect Law (Bažant et al., 1988).

References

Barenblatt, G.I. (1979) **Similarity, Self-Similarity and Intermediate Asymptotics**, Consultant Bureau, New York.

Bažant, Z.P, Kazemi, M.T., Hasegawa, T. and Mazars, J. (1991) Size effect in brazilian split-cylinder tests: measurements and fracture analysis, **ACI Materials Journal**, **88**, 325-332.

Bažant, Z.P, Sener, S. and Prat, P.C. (1988) Size effect test of torsional failure of plain and reiforced concrete beams, **Materials and Structures**, **21**, 425-430.

Carpinteri, A. (1982) Notch sensitivity in fracture testing of aggregative materials, **Engineering Fracture Mechanics**, **16**, 467-481.

Carpinteri, A. (1986) **Mechanical Damage and Crack Growth in Concrete: Plastic Collapse to Brittle Fracture**, Martinus Nijhoff Publishers, Dordrecht.

Carpinteri, A. (1989) Decrease of apparent tensile and bending strength with specimen size: two different explanations based on fracture mechanics, **Int. J. of Solids and Structures**, **25**, 407-429.

Carpinteri, A. (1992) Fractal nature of material microstructure and size effects on apparent mechanical properties, **LFM Internal Report**, **1/92**.

Eligehausen, R., Bouška, P, Červenka, V. and Pukl, R. (1992) Size effect of the concrete cone failure load of anchor bolts, in **Fracture Mechanics of Concrete structures**, Proceedings of 1st FRAMCOS, Breckenridge, pp.517-525.

Falconer, K. (1990) **Fractal Geometry: Mathematical Foundations and Application**, John Wiley & Sons, Chichester.

Freudenthal, A.M. (1968) Statistical approach to brittle fracture, in **Fracture** (ed. H. Liebowitz), **2**, pp.591-619.

Griffith, A.A.(1921) The phenomenon of rupture and flow in solids, **Philosophical Transaction of the Royal Society**, **A221**, London, 136-198.

Hasegawa, T., Shioya, T. and Okada, T. (1985) Size effect on splitting tensile strength of concrete, in **Proceedings of the Japan Concrete Institute 7th Conference**, pp.309-312.

Herrmann, H.J. and Roux, S. (Eds.) (1990) **Statistical Models for the Fracture of Disordered Media**, North-Holland, Amsterdam.

Jayatilaka, A.S. (1979) **Fracture of Engineering Brittle Materials**, Applied Science, London.

Kim, J. and Eo, S. (1990) Size effect in concrete specimens with dissimilar initial cracks, **Magazine of Concrete Research**, **42**, 233-238.

Mandelbrot, B.B. (1982) **The Fractal Geometry of Nature**, W.H. Freeman and Company, New York.

Marquardt, D.W. (1963) An algorithm for least-squares estimation of nonlinear parameters, **J. Soc. Indust. Appl. Math.**, **11**, 431-441.

Sabnis, G.M. and Mirza, S.M. (1979) Size effect in model concretes?, **J. of Structural Division, ASCE**, **105**, 1007-1020.

Tang, T., Shah, S.P. and Ouyang, C. (1992) Fracture mechanics and size effect of concrete in tension, **J. of Structural Division, ASCE**, **118**, 3169-3185.

Weibull, W.(1939) **A Statistical Theory for the Strength of Materials**, Swedish Royal Institute for Engineering Research, Stockholm.

Wilson, K.G. (1971) Renormalization group and critical phenomena, **Physical Review**, **B4**, 3174-3205.

Wilson, K.G. (1979) Problems in physics with many scales of length, **Scientific American** (Italian Edition), **23**, 140-157.

3 TENSION SOFTENING DIAGRAMS AND LONGITUDINALLY REINFORCED BEAMS

B.L. KARIHALOO
School of Civil and Mining Engineering, The University of Sydney, Sydney, Australia

Abstract
This paper will present several two- and three-dimensional micromechanical models for describing the tension softening response of plain concrete. It will be shown that the relationship between the residual stress transfer capability and the crack opening displacement depends on only the fracture toughness of the matrix material (i.e. cement mortar) and the volume fraction of the stiff second phase (i.e. coarse aggregate). The models can therefore also describe the tension softening behaviour of any quasi-brittle material.
The tension softening diagrams are useful not only in studying the fracture process in plain concrete but also in investigating the bond stress transfer from a reinforcing bar to surrounding concrete in reinforced concrete beams. A method for the splitting failure of reinforced concrete beams will be briefly presented and shown to be quite insensitive to the shape of the tension softening diagram. The latter may however play an important role, if the beam is submerged in water.
Keywords: Tension Softening, Plain Concrete, Bond Stress, Reinforced Concrete, Beams, Splitting Failure.

1 Introduction

Plain concrete which has traditionally been regarded as brittle in fact exhibits a moderately strain-hardening behaviour prior to the attainment of its ultimate tensile strength. This behaviour is reminiscent of that of the high strength metals. However, unlike the latter, concrete is characterized by an increase in deformation with decreasing tensile carrying capacity past the ultimate strength, i.e. by tension softening. The tension softening response is a result of the existence of a diffuse zone of microdamage (a process zone).

In this paper we shall first discuss briefly the reasons behind the observed moderate pre-peak nonlinearity of concrete. We shall then consider several two- and three-dimensional micromechanical models for the description of its tension softening behaviour. The decreasing tensile stress transfer capacity with increasing deformation in the tension softening regime is a result of the progressive rupture of the intact ligaments that break the continuity of flaws. In practice for ease of computation, the tension softening relationships determined from micromechanical considerations are approximated by monomial, expo-

Fracture of Brittle Disordered Materials: Concrete, Rock and Ceramics. Edited by G. Baker and B.L. Karihaloo. Published in 1995 by Taylor & Francis, 2 Park Square, Milton Park, Abingdon, Oxon, OX14 4RN. ISBN: 0 419 19050 3.

nential or polynomial functions depending upon the available test data. We shall use such approximate tension softening diagrams for predicting the longitudinal splitting force of a reinforced concrete beam.

2 Pre-peak nonlinear response

Figure 1 illustrates the typical load-deformation response of concrete in tension recorded using a closed-loop testing machine. The post-peak portion of the response curve can only be obtained by controlling a monotonically growing deformation parameter, e.g. crack opening, but not by controlling the force which must decrease.

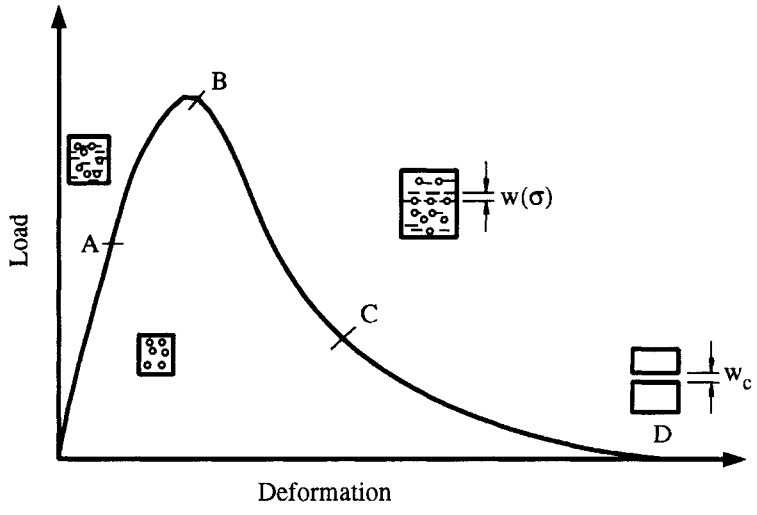

Fig.1 Typical load-deformation response of a quasi-brittle material in tension showing
(i) the transition from linear to nonlinear response (point A);
(ii) pre-peak nonlinearity (AB);
(iii) onset of localization of deformation (point B);
(iv) post-peak tension softening response (BCD)

The pre-peak strain hardening behaviour (stage AB in Fig. 1) is due to diffuse progressive damage of the material under increasing tensile stress as a result of the formation of microcracks along the interfaces between the mortar matrix and coarse aggregate particles and of their deflection into the matrix. The transition from linear to nonlinear response (point A in Fig. 1) is primarily governed by the extent of available interfaces. Kaplan (1963) measured accurately the strain at this transition for concrete under several tensile loading combinations (e.g. direct tension, three-point bending, four-point bending) and found that it depends on only the volume fraction of coarse aggregate in the concrete mix.

The interfacial microcracks first form between the matrix and largest coarse aggregate

particles. With a further increase in tensile stress not only do the existing microcracks propagate stably but also more microcracks are progressively formed at interfaces between the matrix and coarse aggregate particles of smaller sizes. As concrete usually contains a range of sizes, the process of formation, stable growth and deflection of microcracks continues under increasing tensile stress resulting in the pre-peak nonlinearity.

This pre-peak strain hardening behaviour has been successfully explained using the concepts of damage mechanics (Krajcinovic and Fonseka, 1981; Lemaitre, 1985; Karihaloo and Fu, 1989, 1990). Their description is however beyond the scope of this paper.

3 Post-peak tension softening

The microcracks resulting in the pre-peak nonlinearity are not too numerous and the damage is distributed throughout the material. However, when sufficient damage has accumulated a dominant macroflaw localizes along the eventual failure plane (point B in Fig. 1). This macroflaw would lead to immediate fracture in a brittle material. In concrete its immediate catastrophic advance is prevented by mechanisms other than those responsible for pre-peak nonlinearity. The major mechanism is the so-called bridging mechanism which breaks the continuity of the dominant macroflaw so that the (smaller) discontinuous segments can no longer grow unstably. It is however worth noting that the strength of bridging is not by itself enough to allow recording of the tension softening behaviour without a feed-back signal. This control signal is provided by any monotonically increasing deformation but not by the decreasing force.

The bridging is provided by the interlocking of coarse aggregate particles, by the strain hardening capacity of unbroken ligaments between macrocrack segments and by any voids which attract and trap macrocracks. Several two- and three-dimensional tension softening models have been proposed, and we will now consider these.

3.1 Two-dimensional models

A two-dimensional tension softening model was proposed by Horii *et al.* (1987) and by Ortiz (1988). In this model, the discontinuous macroflaw is regarded as an infinite row of collinear cracks separated by uncracked material ligaments. The cracks are assumed to lie along the eventual failure plane and the mechanics of their growth is studied under a normal tensile stress σ which is assumed to be well removed from the crack plane . At the onset of tension softening (point B in Fig. 1) each segment of the discontinuous macroflaw is of size $2\ell_0$ and is separated from the neighbouring segment by an uncracked ligament of length (d - $2\ell_0$), so that $2\ell_0/d = \gamma_0$ may be regarded as the (small) accumulated damage per unit area (volume) at this instant. To study the tension softening response we need to know how the tensile stress transfer capability σ decreases as the uncracked ligaments progressively break so that the relative cracked area increases until eventually rupture occurs. Each cracked segment of the discontinuous macroflaw will grow when the stress intensity factor which will be the same at either tip, reaches the intrinsic matrix critical stress intensity factor K_{Ic}^m (i.e. the fracture toughness of cement mortar which is regarded as a material constant).

This two-dimensional model predicts that past a certain maximum value the inelastic

deformation must also decrease with the stress in order to satisfy the crack growth criterion $K_I = K_{Ic}^m$ along the tension softening curve. Such an unexpected and unstable situation should not however be confused with the response of real material. In fact, it was to be expected from this model, because of the assumption that the cracked segments will grow until they coalesce and result in complete rupture. A proper stability analysis of this model however shows (Melin, 1983) that when the tips of adjacent straight cracks approach so close to each other that their straight paths would be unstable, they would avoid each other by curving and form "eyelets". Such crack curving and formation of eyelets have been repeatedly observed in tensile tests on cement mortar and concrete (van Mier and Vonk, 1991).

The tension softening response of concrete is generally characterized by a pronounced tail (Reinhardt *et al.*, 1986), i.e. a relatively large value of critical crack opening displacement w_c at rupture, without the instability predicted by the foregoing two-dimensional model. There could be many reasons for the observed pronounced tail. For instance, it could be the result of the presence of pores in the material because they are known to attract and arrest cracks. It could be because the fragmented macroflaw does not lie in one plane but in a thick band such that the failure can only occur when the cracks in neighbouring planes are connected by diagonal cracks. In the next two- dimensional model we shall only explore the first possibility in an approximate manner.

We shall assume for simplicity that at the onset of tension softening the discontinuous macroflaw consists of a row of collinear cracks separated not only by uncracked material ligaments, as in the preceding model, but also by circular pores. The latter, it will be noticed, add a certain "thickness" to the eventual failure plane. At the onset of tension softening each segment of the discontinuous macroflaw in this model (Fig. 2) is assumed to consist of cracks of length $2\ell_0$ interspersed by circular pores of diameter $2a_0$, such that the initial "thickness" of the eventual failure band also equals $2a_0$. The neighbouring segments are separated by uncracked ligaments each of length $d - 2(a_0 + \ell_0)$, so that now $2(a_0+\ell_0)/d = \gamma_0$ is the accumulated damage per unit area (volume) at the onset of tension softening.

The mathematical problem corresponding to the assumed tension softening model consists of an infinite row of collinear circular holes with edge cracks subjected to a remote tensile stress σ. It has been solved by Karihaloo *et al.* (1991). Unlike the preceding problem, the solution is not available in an analytical form. However, the numerical results for the stress intensity factor K_I at each crack tip in the infinite row and for the opening displacement of each macroflaw segment $[v]$ have been fitted by polynomial approximations. We shall only present the polynomial approximations for K_I and $[v]$ without going into detail.

K_I at each crack tip in the row is given by

$$K_I = \sigma\sqrt{\pi(a+\ell)}\, f(\beta,\gamma), \tag{1}$$

where

$$f(\beta,\gamma) = \left(1 + \sum_{r=1}^{3}\sum_{s=0}^{3} C_{rs}\beta^r\gamma^s\right)\left(\frac{\tan\pi\gamma/2}{\pi\gamma/2}\right)^{\frac{1}{2}}, \tag{2}$$

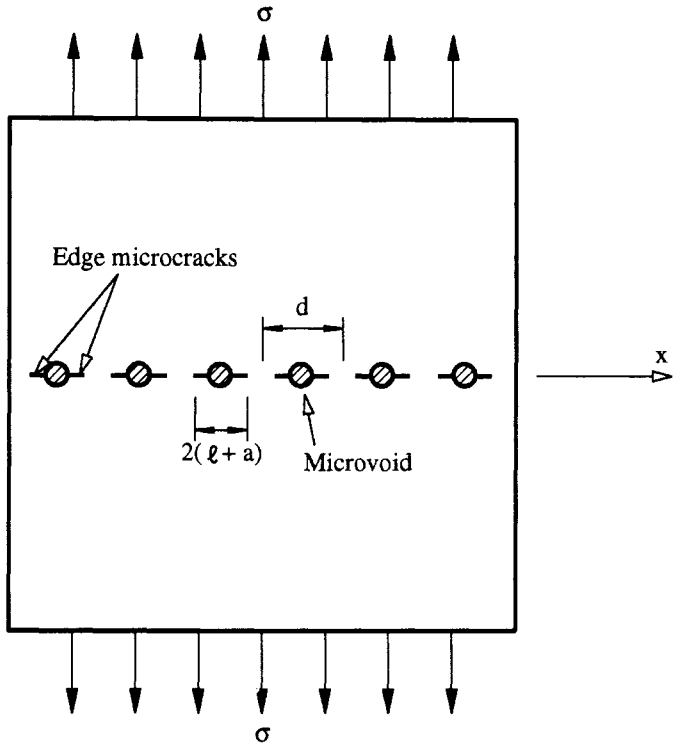

Fig.2 Tension softening model in which the discontinuous macroflaw is modelled by microvoids with edge microcracks interspersed by unbroken ligaments

with $\beta = a/(a + \ell)$ and $\gamma = 2(a + \ell)/d$. The coefficients C_{rs} are listed in Table 1. It is noted that the polynomial approximation (2) differs from the numerical values by less than 0.7%. It was deliberately chosen in the form (2) in order to be able to recover easily the exact analytical result of the preceding model by setting $a = 0$, i.e. $\beta = 0$. When this is done, (2) reduces to

$$f(0,\gamma) = \left[\frac{\tan \pi\gamma/2}{\pi\gamma/2}\right]^{\frac{1}{2}}, \tag{3}$$

which when substituted into eqn (1), together with $a = 0$, indeed reproduces the exact result. We impose now the crack growth criterion in the tension softening regime, namely $K_I = K_{Ic}^m$, and get the following relation between σ and f_t

$$\frac{\sigma}{f_t} = \sqrt{\frac{(a_0 + \ell_0)}{(a + \ell)}\,\frac{f(\beta_0,\gamma_0)}{f(\beta,\gamma)}}, \tag{4}$$

where β_0 and γ_0 refer to the values of β and γ, respectively at the onset of tension softening.

Next, we report the polynomial approximation for the average opening of macrocrack segment $[v]$. We note first that the solution of the mathematical problem exploited the periodicity of circular holes with edge cracks, so that it was only necessary to solve over a quadrant after imposing the appropriate stress and displacement conditions. Note that over the quadrant of the hole, the total opening is $v^+(x) + \sqrt{a^2 - x^2}$ $(0 \leq x \leq a)$, where $v^+(x)$ refers to the opening displacement of the upper right quadrant of the flaw segment.

The average opening of each flaw segment over the period d to account for the unbroken bridging ligaments is

$$w_t = \frac{\sigma d}{2E'} g(\beta, \gamma), \tag{5}$$

where the best-fit polynomial approximation $g(\beta, \gamma)$ to the numerical results is

$$g(\beta, \gamma) = \left(1 + \frac{1}{\sqrt{1-\gamma}} \sum_{r=1}^{3} \sum_{s=0}^{3} D_{rs} \beta^r \gamma^s\right) \left(\frac{8}{\pi} \log(\sec \frac{\pi \gamma}{2})\right). \tag{6}$$

The coefficients D_{rs} are listed in Table 1.

Table 1. Coefficients C_{rs} and D_{rs} in the polynomial approximations (2) and (6)

r	s	C_{rs}	D_{rs}
1	0	-0.0131246	1.0012000
1	1	-0.1801658	-0.8720340
1	2	0.3349874	0.5115431
1	3	1.3436450	0.8064520
2	0	0.6175492	-1.1061990
2	1	0.8620229	1.1268440
2	2	-2.0971480	-2.4623200
2	3	-3.1807730	-1.3658990
3	0	-0.8855224	0.4455536
3	1	-0.5714183	-0.7251084
3	2	0.8950143	2.4867950
3	3	3.0786150	0.5254524

The polynomial approximation was again deliberately chosen in the form (6) with a view to recovering the result of the preceding model, when $a = 0$. It differs from the numerical values by less than 3%, except near the termination of tension softening ($\gamma \to 1$) when the error increases to about 6.3%.

The net inelastic deformation in the tension softening regime is given by

$$\frac{w}{w_0} = \frac{\sigma}{f_t} \left[\frac{g(\beta, \gamma)}{g(\beta_0, \gamma_0)}\right] - 1. \tag{7}$$

In the present model, the tension softening relation between the residual tensile carrying capacity σ and the inelastic deformation w is given by eqns (4) and (7). In addition to the two material parameters γ_0 and K_{Ic}^m of the previous model, it contains the parameter β which is a measure of the relative fractions of microvoids and microcracks in the localized

deformation band. Thus $\beta = 0$ denotes absence of any microvoids, whereas $\beta \approx 1$ implies microvoids with negligibly small edge cracks. Note that for the validity of the present model edge cracks however small, must be present. It is not valid when no edge cracks are present ($\beta = 1$).

The tension softening diagrams for three values of ℓ/a and several values of γ_0 are shown in Fig. 3. The curves in Fig. 3a for $\ell/a = 10$ (or $\beta = 1/11$) are already very nearly the same as for $\beta = 0$ and exhibit the same unstable behaviour.

As β increases, not only does the critical value of crack tip opening displacement w_c increase, but, more importantly, the failure is less unstable. In fact, at $\ell/a = 0.1$ (Fig. 3c) the unstable branch is totally absent, confirming the stabilizing role of voids in the tension softening process. To illustrate this, we now show that the present model indeed predicts that $w \to \infty$ as $\gamma \to 1$ at complete rupture. For this, it is convenient to rewrite eqn (7), using eqn (4), in the following form

$$\frac{wE'}{f_t d} = \frac{f(\beta_0, \gamma_0)}{2} \left[\left(\frac{\gamma_0}{\gamma} \right)^{\frac{1}{2}} \frac{g(\beta, \gamma)}{f(\beta, \gamma)} - \frac{g(\beta_0, \gamma_0)}{f(\beta_0, \gamma_0)} \right]. \tag{8}$$

Substituting (2) and (6) into (8) and taking the limit as $\gamma \to 1$, we find that for β greater than 0, $g(\beta, \gamma)/f(\beta, \gamma) \to \infty$, whereas when $\beta = 0$, $g(0, \gamma)/f(0, \gamma) \to 0$, thereby confirming the instability inherent in the preceding collinear crack model.

It should be mentioned that tension softening models cannot predict the exact value of the critical crack opening at rupture ($\gamma = 1$). A notional value may be used by limiting γ to 1 - δ with δ governed by the frictional pull-out characteristics of coarse aggregate from the cement mortar matrix.

Another two-dimensional model, proposed by Li and Huang (1990) assumes that the tensile strength of concrete is limited by the branching of the largest interfacial crack into the matrix which then becomes the dominant discontinuous macroflaw. The latter subsequently propagates into a "homogeneous" material with a fracture toughness which reflects the distribution of interfacial cracks and the possible deflection of the macroflaw when it meets hard second phase particles.

The tension softening curve according to this model is

$$w = \frac{(K_{Ic}^{hom})^2}{E'(1 - V_f) f_t} \frac{1}{(\sigma/f_t)} \left[1 - \left(\frac{\sigma}{f_t} \right)^3 \right], \tag{9}$$

where V_f is the volume fraction of coarse aggregate in the mix.

As with the second model described above, the $w - \sigma$ curve as expressed by eqn (9) exhibits a long tail decaying indefinitely to $\sigma = 0$, as $w \to \infty$. In reality though, a frictional pull-out mode takes over whereby the hard second phase particles even after being completely debonded from the matrix are prevented from pull-out by friction.

To complete the description of this model, let us make a few observations on the calculation of the fracture toughness K_{Ic}^{hom} of the "homogenized" medium. When the dominant macroflaw along the interface between the largest coarse aggregate particles and matrix grows and encounters another particle it is most likely to deflect around this

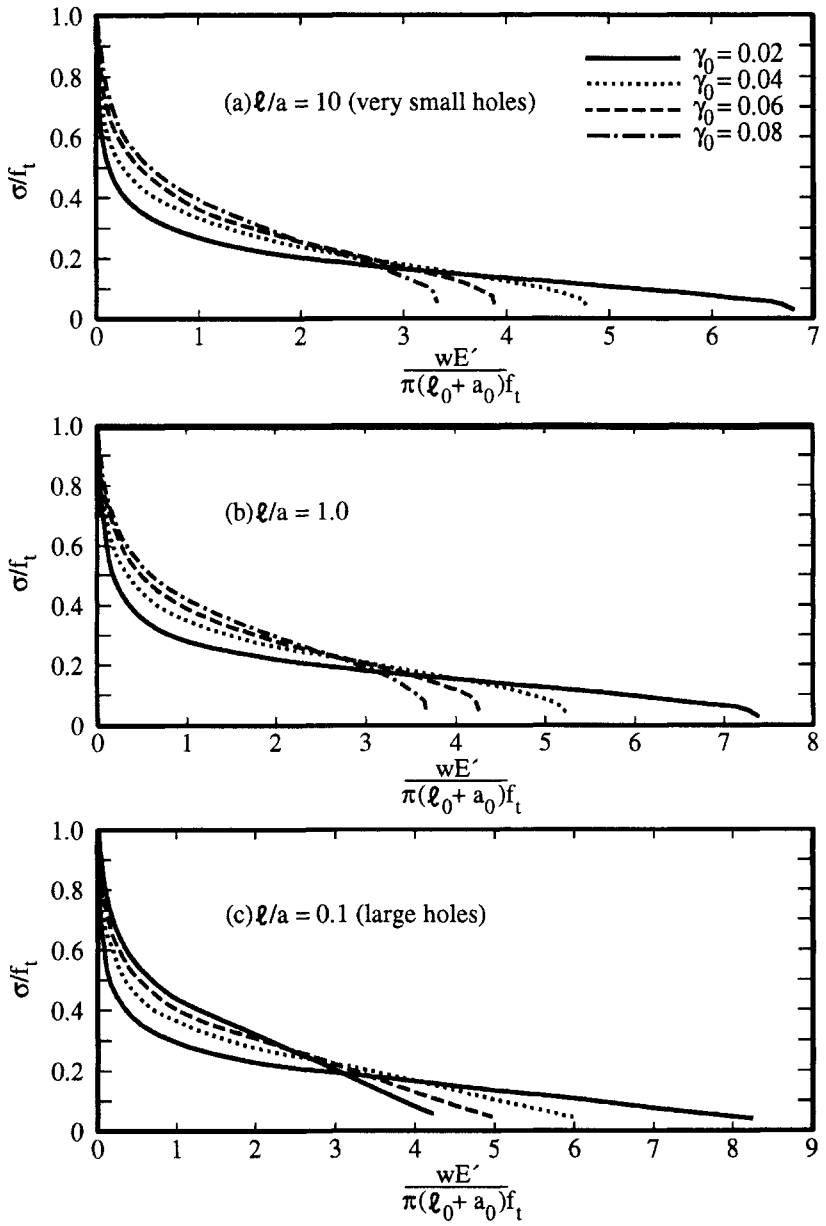

Fig.3 Tension softening curves predicted by the model shown in Fig.2

particle because the matrix-particle interface is usually weak. This deflection reduces the stress intensity factor at the new crack tip because the latter is no longer oriented normal to the applied tensile stress. Thus the material is effectively toughened. In addition to crack deflection toughening, the presence of microcracks at the matrix-particle interfaces reduces the elastic modulus of the material ahead of the dominant macroflaw leading to a shielding effect whereby its tip "feels" a reduced stress intensity factor. The separate analysis of these two toughening mechanisms is beyond the scope of the present paper. Suffice it to say that such an analysis allows us explicitly to relate the second phase volume fraction to the fracture toughness increment over and above the matrix fracture toughness. The interested reader will find the details in Li and Huang (1990). Here, we just report the final result

$$\frac{K_{Ic}^{hom}}{K_{Ic}^{m}} = \left[\frac{1.0 + 0.87V_f}{1 - \frac{\pi^2}{16} V_f(1-\nu^2)}\right]^{\frac{1}{2}}. \tag{10}$$

For $\nu = 0.25$, and $V_f = 0.1, 0.3, 0.5$, and 0.7, the fracture toughness of the "homogenized" material is 7, 23, 41, and 64% higher than the matrix fracture toughness.

3.2 Three-dimensional model

The two-dimensional models studied above predict a rather sudden drop in the tensile carrying capacity immediately after the onset of tension softening. This may partly be a consequence of the two-dimensionality of the models. The constraint provided by the thickness direction may indeed result in a more gradual reduction in the initial post-peak tensile carrying capacity. To verify this, we shall now consider a three-dimensional analog of the two-dimensional collinear crack model for which results are available (Huang and Karihaloo, 1992). In this three-dimensional model, the discontinuous macroflaw is modelled by a doubly periodic array of penny-shaped (circular) cracks (period = ℓ) in the eventual failure plane (Fig. 4). For simplicity the cracks are assumed to be of identical size (radius = a) and to grow in a self-similar manner under a remote normal tensile stress σ until the neighbouring cracks touch one another (i.e. $\ell = 2a$). At that instant the degree of damage in the material $\gamma = \pi a^2/\ell^2$ takes the value $\pi/4$. Because of severe mathematical difficulties associated with the study of overlapping circular cracks, the analysis has not been carried to complete rupture when $\gamma = 1$. Nevertheless, the limited analysis that has been performed gives a good indication of the constraint provided by the third dimension.

The mathematical problem corresponding to the above model has been solved by two methods. Both methods require the numerical solution of a system of integral equations. The first method does not involve any approximations and thus suffers from slow convergence, especially as $\gamma \to \pi/4$. To improve the rate of convergence without at the same time unduly sacrificing the accuracy of results, a key assumption akin to the Saint Venant approximation in the Theory of Elasticity is made in the second method. The key assumption is that the difference between the actual opening displacement of any one crack in the array and the average opening displacement of all the remaining cracks is so small as to be ignored. This allows the reduction of the governing integral equations to highly convergent ones even at the instant when the neighbouring cracks come in contact (i.e. γ

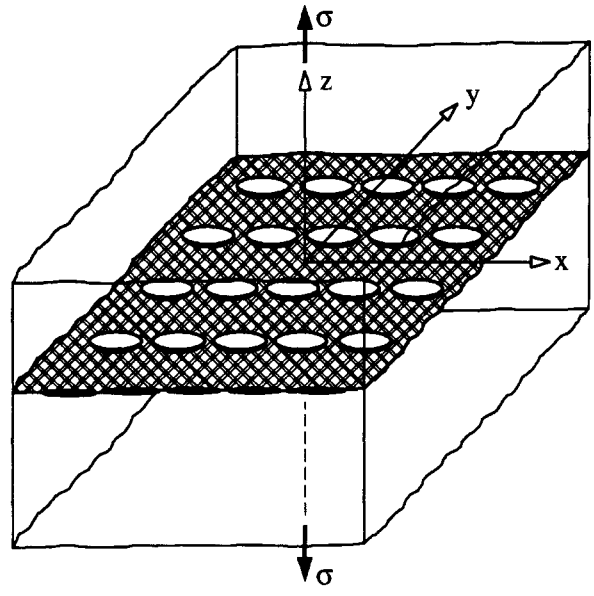

Fig.4 A doubly periodic array of square penny-shaped cracks along the eventual fracture plane (z = 0)

$= \pi/4$).

We shall omit details of mathematical formulation and solution procedure and only present the results that parallel those of the corresponding two-dimensional model. However, we can no longer talk about crack tips, but have to consider the whole circumference of the circular crack. The stress intensity factor along the circumference (the edge) varies with the polar angle ϕ measured from the positive x-axis in the eventual failure plane, i.e. $z = 0$ (Fig. 4). It is maximum at the poles $\phi = 0$, $\pi/2$, π, and $3\pi/2$, so that the crack growth criterion now has to be applied to the average stress intensity factor along the edge, i.e. $\overline{K_I} = K_{Ic}^m$. As with the two-dimensional model, we shall relate $\overline{K_I}$ to the average crack opening volume.

The results corresponding to the two-dimensional model are

$$\frac{\sigma}{f_t} = \left(\frac{\gamma_0}{\gamma}\right)^{\frac{1}{4}} \frac{f(\gamma_0)}{f(\gamma)}, \tag{11}$$

$$\frac{3wE'}{16a_0 f_t} = \frac{g(\gamma_0)}{\sqrt{\gamma_0}} \left(\frac{\sigma}{f_t} \frac{g(\gamma)}{g(\gamma_0)} - 1\right), \tag{12}$$

where $\gamma_0 = \pi(a_0/\ell)^2$ and $f_t = \pi K_{Ic}^m / [\sqrt{2a_0}\, f(\gamma_0)]$.

As before, the numerical values of $f(\gamma)$ and $g(\gamma)$ have been fitted with polynomial approximations chosen such that as $\ell/(2a) \to \infty$, the results for a solitary circular crack under a uniform normal tension are retrieved

$$f(\gamma) = 1 + \sqrt{\log \sec(\frac{\pi}{2}\gamma)} \sum_{r=1}^{5} C_r \gamma^r \tag{13}$$

$$g(\gamma) = \gamma^{\frac{3}{2}} \sum_{r=1}^{5} D_r \gamma^{r-1}. \tag{14}$$

The coefficients C_r and D_r are listed in Table 2.

Table 2. Coefficients C_r and D_r in the polynomial approximations (13) and (14)

r	C_r	D_r
1	2.2649	0.3224
2	-19.7365	-0.1192
3	82.8536	1.1977
4	-142.0318	-2.6264
5	85.0150	2.1644

The error in the polynomial approximation (13) for the dimensionless average stress intensity factor is less than 4.7% over the range $0.02 \leq \gamma \leq \pi/4$, whereas that of the polynomial approximation (14) for the dimensionless average crack opening volume is less than 1.05% over the same range.

The tension softening curves determined by (11) and (12) are shown in Fig. 5 for several values of the accumulated damage at the onset of tension softening. A comparison of these curves with those on Fig. 3a clearly shows that the tri-axiality does indeed produce a more gradual loss in the tensile carrying capacity immediately after the onset of tension softening. In comparing the curves on Figs. 3a and 5, the differences in the horizontal scales ought to be borne in mind.

The solution of the above three-dimensional model requires the summation of doubly-infinite series, resulting from the consideration of multiple interactions among all the cracks in the doubly-periodic array. If only the first-order interactions among the cracks are retained, the solution can be considerably simplified because the series can be summed analytically by the application of the mean value theorem. This first order approximation can be expected to be reasonably accurate when the cracks are well apart, i.e. when γ is small. It has the advantage that it can be readily extended to the more general array configuration shown in Fig. 6 (and not only to the array considered above for which $\alpha = \pi/2$), thereby providing an indication of the dependence of $f(\gamma)$ and $g(\gamma)$ on the geometry of the array, in addition to their primary dependence on the cracked area fraction γ. This has been investigated by Huang *et al.* (1993) who found that the initial stage of the tension softening curve is not particularly sensitive to the distribution of discontinuous macroflaws in the eventual fracture plane.

In practice for ease of computation, the tension softening curves for concrete are approximated by monomial (Reinhardt, 1984), exponential (Reinhardt *et al.*, 1986) or

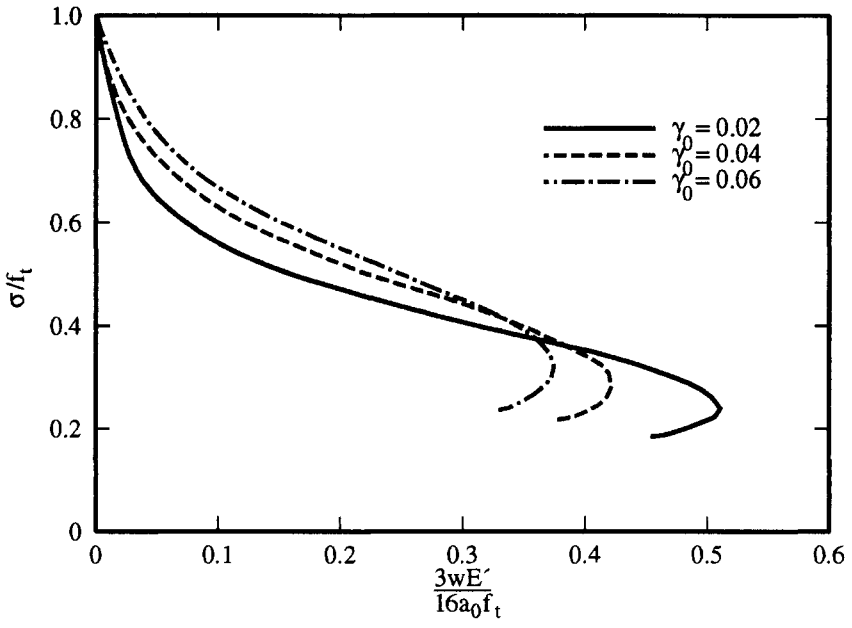

Fig.5 Tension softening curves for the doubly periodic array of Fig.4

polynomial (Karihaloo and Nallathambi, 1989) functions depending on the available test data. We shall demonstrate the use of these approximate functions in the next section for the determination of the longitudinal splitting force in a reinforced concrete beam.

4 Splitting failure of longitudinally reinforced concrete beams

When a deformed reinforcing bar surrounded by concrete is pulled, movement of the steel ribs will be resisted by concrete. Large inclined compressive forces will radiate from the ribs to the surrounding concrete giving rise to circumferential forces in the latter (Fig. 7). Tepfers (1979) assumed that this radial component of bond stress can be considered as hydrostatic pressure acting on a thick-walled concrete ring, and concrete will crack if the induced stress reaches its tensile capacity. However, the maximum pull-out force is reached only when the cracks penetrate some distance into the material. Hence, the concrete ring will be comprised of an outer elastic part surrounding an inner cracked part at failure. The ultimate bond stress is therefore given by superposition of the contributions from the individual parts of the ring, i.e. $U_{ult} = U_{e,ult} + U_{c,ult}$.

The contribution of the elastic part $U_{e,ult}$ of the concrete ring is calculated using the elastic the elastic theory. For the cracked part of the concrete ring, if compatibility at the interface between the cracked and uncracked parts (Fig. 8) is cinsidered, the total elongation at that section can be expressed in terms of the number and width of

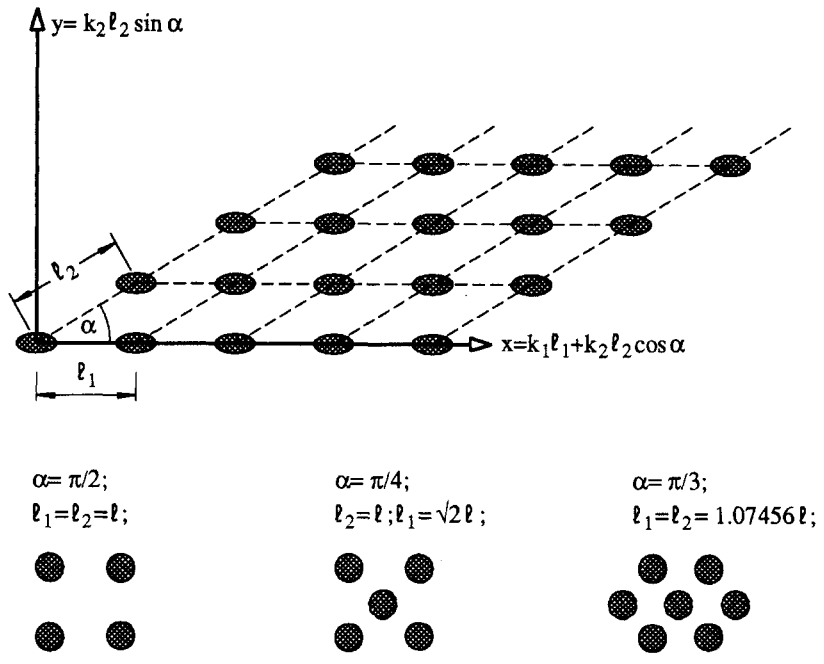

Fig.6 Various doubly periodic arrays with different distribution angle α

cracks. When the power function relation for the tension softening of concrete proposed by Reinhardt (1984)

$$\frac{\sigma}{f_t} = 1 - \left(\frac{w}{w_c}\right)^{0.248} \tag{15}$$

is substituted, the stress for a finite section in the cracked part is obtained. On integration, the force and hence the bond resistance contributed by the cracked part of the ring can be calculated. The tension softening curve (15) predicts a sudden stress drop at small w as compared with the test results. To overcome this deficiency, Reinhardt *et al.* (1986) later proposed a more complicated relationship in the form

$$\frac{\sigma}{f_t} = [1 + (C_1\frac{w}{w_c})^3]\exp(-C_2\frac{w}{w_c}) - \frac{w}{w_c}(1 + C_1^3)\exp(-C_2), \tag{16}$$

where $C_1 = 3$ and $C_2 = 6.93$. However, as this approximate relationship still has a finite slope when w approaches w_c, Karihaloo and Nallathambi (1989) proposed the following approximation

$$\frac{\sigma}{f_t} = 1 - 9.2431(\frac{w}{w_c})^2 + 33.8259(\frac{w}{w_c})^3 - 59.4248(\frac{w}{w_c})^4$$